Nonlocal van der Waals functionals for solids: Choosing an appropriate one

Fabien Tran,[1] Leila Kalantari,[1] Boubacar Traoré,[2] Xavier Rocquefelte,[3] and Peter Blaha[1]
[1]*Institute of Materials Chemistry, Vienna University of Technology, Getreidemarkt 9/165-TC, A-1060 Vienna, Austria*
[2]*Univ Rennes, INSA Rennes, CNRS, Institut FOTON - UMR 6082, F-35000 Rennes, France*
[3]*Univ Rennes, ENSCR, INSA Rennes, CNRS, ISCR (Institut des Sciences Chimiques de Rennes) - UMR 6226, F-35000 Rennes, France*

(Received 1 March 2019; revised manuscript received 6 May 2019; published 5 June 2019)

The nonlocal van der Waals (NL-vdW) functionals [M. Dion *et al.*, Phys. Rev. Lett. **92**, 246401 (2004)] are being applied more and more frequently in solid-state physics, since they have shown to be much more reliable than the traditional semilocal functionals for systems in which weak interactions play a major role. However, a certain number of NL-vdW functionals have been proposed during the last few years, such that it is not always clear which one should be used. In this work, an assessment of NL-vdW functionals is presented. Our test set consists of weakly bound solids, namely rare gases, layered systems such as graphite, and molecular solids, but also strongly bound solids in order to provide a more general conclusion about the accuracy of NL-vdW functionals for extended systems. We found that among the tested functionals, rev-vdW-DF2 [I. Hamada, Phys. Rev. B **89**, 121103(R) (2014)] is very accurate for weakly bound solids, but also quite reliable for strongly bound solids.

DOI: 10.1103/PhysRevMaterials.3.063602

I. INTRODUCTION

The pioneering works of Langreth, Lundqvist, and coworkers on nonlocal van der Waals functionals [1–6] (abbreviated as NL-vdW) have contributed significantly in making density functional theory [7,8] (DFT) much more accurate for extended systems in which the weak vdW interactions are important. Before the advent of the NL-vdW functionals and atom-pairwise methods [9–11] (see Refs. [12,13] for reviews), the DFT calculations with periodic boundary conditions were done mostly with the local density approximation (LDA) [8] or generalized gradient approximation (GGA) [14]. However, since the physics of the London dispersion forces is included neither in LDA and GGA nor in meta-GGA (MGGA) and hybrid functionals, all these methods are in general quite unreliable for the calculation of the length and binding energy of noncovalent bonds.

Thus, the NL-vdW methods, the focus of this work, are becoming increasingly popular, and particularly in the solid-state community [15] thanks to the availability of computationally fast implementations [16–20]. However, since there is still no full confidence in the accuracy of the results when using a NL-vdW functional (the so-called chemical accuracy of 1 kcal/mol can sometimes be reached, but not systematically; see, e.g., Refs. [21,22]), new ones are constantly being proposed and currently more than twenty exist (see, e.g., Refs. [23–26]). Consequently, as in the case of semilocal (i.e., GGA and MGGA) and hybrid functionals, there is a rather large freedom in the choice of the NL-vdW functional and it may not be always clear which one to choose.

In our previous work [27], a plethora of functionals of the first four rungs of DFT Jacob's ladder [28] were tested on a set consisting of strongly bound and weakly bound solids. Functionals including a term of the atom-pairwise type to account for the vdW interactions, DFT + D3 (Ref. [11]) and DFT+D3(BJ) (Ref. [29]), were also considered. Here, we extend this comparison by considering NL-vdW functionals, not considered in Ref. [27], and the main goal is to provide a useful summary of their performance for the geometry and binding energy of periodic solids.

Additionally, results for the binding energy of molecules will also be shown in order to provide a hint on the performance of the tested functionals on finite systems.

The paper is organized as follows. Section II gives details about the methods. Then, the results are presented and discussed in Sec. III and summarized in Sec. IV.

II. METHODS

In NL-vdW methods [2], the exchange-correlation (xc) functional is given by

$$E_{\rm xc} = E_{\rm xc}^{\rm SL/hybrid} + E_{\rm c,disp}^{\rm NL}, \tag{1}$$

where the first term is of the semilocal (SL) or hybrid [30,31] type and the second term reads

$$E_{\rm c,disp}^{\rm NL} = \frac{1}{2}\iint \rho(\boldsymbol{r}_1)\Phi(\boldsymbol{r}_1,\boldsymbol{r}_2)\rho(\boldsymbol{r}_2)d^3r_1 d^3r_2. \tag{2}$$

Thanks to its form, the additional correlation term given by Eq. (2) is able to account for long-range interactions in the system; the specificity of $E_{\rm c,disp}^{\rm NL}$ is to contribute to the binding energy between two systems A and B even when there is no density overlap [i.e., $\rho_{\rm A}(\boldsymbol{r})\rho_{\rm B}(\boldsymbol{r}) = 0\ \forall \boldsymbol{r}$], while in such a case the contribution from $E_{\rm xc}^{\rm SL/hybrid}$ is strictly zero (if we neglect the change in the shape of $\rho_{\rm A}$ and $\rho_{\rm B}$ when the system A-B is formed). The kernel Φ in Eq. (2) depends on the electron density ρ, its derivative $\nabla\rho$, and the interelectronic distance $|\boldsymbol{r}_1 - \boldsymbol{r}_2|$. To our knowledge, five different analytical forms for Φ have been proposed to date [2,32–35], while numerous

reoptimizations of the parameters in Φ have been reported [24,26,36–39].

The choice of the semilocal or hybrid functional $E_{\rm xc}^{\rm SL/hybrid}$ in Eq. (1) is also of crucial importance, since this is of course the total xc functional that has to be accurate. In particular, an important requirement is that $E_{\rm xc}^{\rm SL/hybrid}$ alone should not already lead to an overbinding; otherwise adding $E_{\rm c,disp}^{\rm NL}$ can only make the results worse. Thus, the combination $E_{\rm xc}^{\rm SL/hybrid} + E_{\rm c,disp}^{\rm NL}$ has to be well balanced in order to provide accurate geometry and binding energy [23,25,36,40].

Among the NL-vdW functionals that are available in the literature, a certain number of them were selected for the present work. However, we did not consider NL-vdW functionals based on hybrid functionals [37,38,41,42], since they lead to calculations that are much more expensive, especially for solids. They are therefore less interesting from a practical point of view as long as the electronic structure is of no particular interest. Thus, only semilocal-based NL-vdW functionals are considered and now listed.

The functional vdW-DF from Dion *et al.* (DRSLL) [2], the first proposed NL-vdW functional that can be applied to systems with arbitrary geometry, consists of the GGA exchange revPBE [43] (a reoptimization of PBE [14]) and LDA correlation [44,45] for the semilocal part. The nonlocal term, Eq. (2), of the vdW-DF functional (DRSLL kernel Φ) has subsequently been used in combination with other semilocal components, and among them, those that are considered in the present work are the following four: C09-vdW from Cooper [46], which uses a GGA (C09x) for exchange and LDA for correlation; optB88-vdW and optB86b-vdW, which are two of the functionals developed by Klimeš *et al.* [21,23] and use for the semilocal component the GGAs optB88 and optB86b for exchange and LDA for correlation (note that optB88 and optB86b are reoptimizations of B88 [47] and B86b [48], respectively), and vdW-DF-cx from Berland and Hyldgaard [25], which consists of a GGA exchange component, LV-PW86r, that is combined with LDA correlation and was constructed to be more consistent with the DRSLL kernel.

The functional vdW-DF2 from Lee *et al.* (LMKLL) [36] uses the GGA exchange PW86R [36] (a reoptimization of PW86 [49]) and LDA for correlation, while the kernel Φ (called LMKLL) in $E_{\rm c,disp}^{\rm NL}$ has the same analytical form as the original DRSLL kernel, but with a reoptimized parameter Z_{ab} ($Z_{ab} = -0.8491$ in DRSLL and $Z_{ab} = -1.887$ in LMKLL). Hamada [40] proposed a revised vdW-DF2 (rev-vdW-DF2) that combines the GGA B86R for exchange (another reoptimization of B86b [48]) and LDA correlation with the LMKLL kernel.

Based on a kernel Φ that has a different analytical form, rVV10 [34] consists of PW86R (exchange) and PBE (correlation) for the semilocal component. Note that the rVV10 kernel is based on the VV10 kernel of Vydrov and Van Voorhis [33] and was made suitable for the method of Román-Pérez and Soler [16] (RPS) to calculate Eq. (2). Also tested are SCAN+rVV10 and PBE+rVV10L from Peng *et al.* [26,39], where the MGGA SCAN [50] and GGA PBE [14] are supplemented by the NL-vdW term rVV10, but with reoptimizations of the parameter b ($b = 6.3$, 15.7, and 10 in rVV10, SCAN+rVV10, and PBE+rVV10L, respectively).

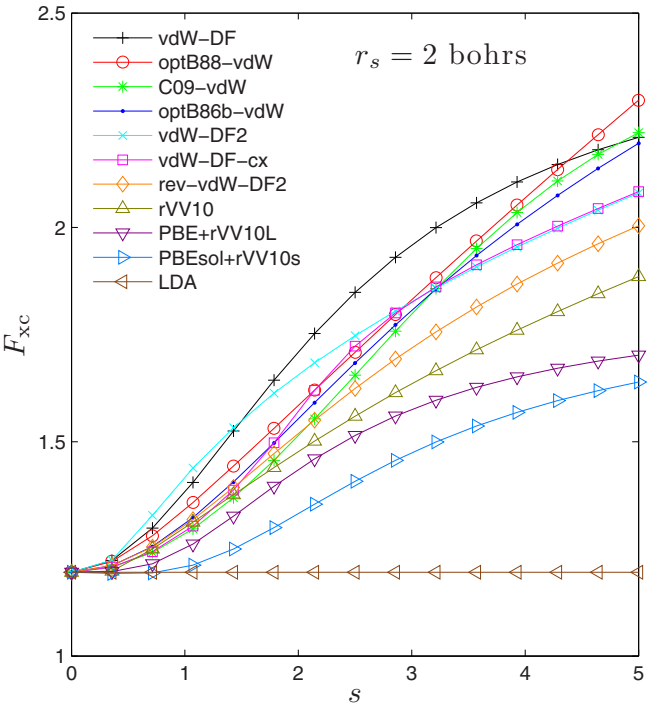

FIG. 1. GGA Enhancement factor $F_{\rm xc}$ of the semilocal component of the NL-vdW functionals plotted as a function of s for $r_s = 2$ bohrs. LDA is also shown.

Note that the rVV10 kernel contains another parameter, C, whose original value (0.0093) was kept in SCAN+rVV10 and PBE+rVV10L.

Finally, the PBEsol+rVV10s functional proposed very recently by Terentjev *et al.* [35] will also be considered. PBEsol+rVV10s uses the PBEsol GGA functional [51] for $E_{\rm xc}^{\rm SL}$ and a modified rVV10 kernel (rVV10s), where $b = 10$ (as in PBE+rVV10L) and C is replaced by a function of the reduced density gradient $s = |\nabla\rho|/[2(3\pi^2)^{1/3}\rho^{4/3}]$:

$$C(s) = C_0 + \frac{C_1}{1 + C_2\left(s - \frac{1}{2}\right)^2}, \tag{3}$$

where $C_0 = 0.0093$, $C_1 = 0.5$, and $C_2 = 300$.

For the sake of comparison, results obtained with LDA, the GGAs PBE and PBEsol, the MGGAs SCAN and TM [52], as well as two atom-pairwise DFT+D3(BJ) methods (PBE-D3(BJ) and revPBE-D3(BJ) [29], including the three-body nonadditive dispersion term [11]) will also be shown. SCAN and TM are modern functionals that have been shown to be overall more accurate than GGA functionals [27,53–60].

The NL-vdW functionals considered here do not constitute an exhaustive list (a few other nonhybrids can be found in Refs. [23,24,61,62]); however they should represent most trends in the results that may be obtained with this group of functionals.

Figure 1 shows the enhancement factor of the semilocal component of the GGA-based NL-vdW functionals, which is defined as the ratio between a GGA xc-energy density $\epsilon_{\rm xc}^{\rm GGA}$

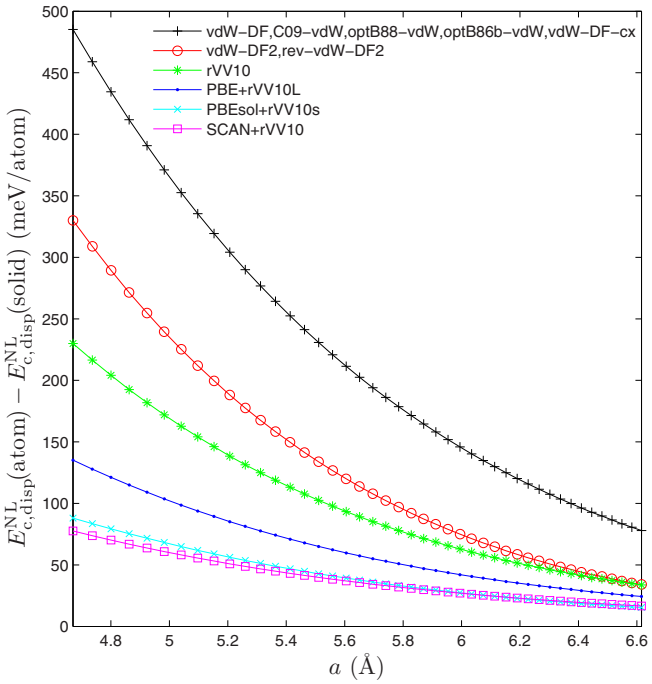

FIG. 2. Contribution to the cohesive energy of Ar coming from the NL dispersion term plotted as a function of the lattice constant. This is shown for all six different kernels considered in this work.

and the LDA exchange-only ϵ_x^{LDA}:

$$F_{xc}(r_s(\boldsymbol{r}), s(\boldsymbol{r})) = \frac{\epsilon_{xc}^{GGA}(\boldsymbol{r})}{\epsilon_x^{LDA}(\boldsymbol{r})}. \quad (4)$$

The functions F_{xc} are plotted as functions of s for a value of $r_s = 2$ bohrs, where $r_s = [3/(4\pi\rho)]^{1/3}$ is the Wigner-Seitz radius. This comparison of the enhancement factors will be useful later when discussing the trends in the results, in particular for strongly bound systems in which the dispersion term does not play a major role.

All six variants of the nonlocal dispersion term [Eq. (2)] considered in this work are compared in Fig. 2, which shows the contribution $E^{NL}_{c,disp}(\text{atom}) - E^{NL}_{c,disp}(\text{solid})$ to the cohesive energy E_{coh} of solid Ar (positive values correspond to binding). Since $E^{NL}_{c,disp}$ represents mainly the dispersion, which is attractive, the curves in Fig. 2 are positive (stronger bonding) and have a negative slope (which favors shorter bond lengths). It can be seen that the magnitude varies dramatically among the different expressions for Eq. (2). The original DRSLL kernel Φ, which is used in five of the functionals, leads to a contribution to E_{coh} that is the largest and one order of magnitude larger than with the two rVV10-type kernels used in PBEsol+rVV10s and SCAN+rVV10. Since the curve with the steepest slope is also obtained with the DRSLL kernel, the effect on the bond length should also be the largest when using this kernel. We mention that the ordering of the curves observed for Ar should remain the same for all or at least most other systems.

The calculations on periodic solids were done with the WIEN2K code [63], which is a full-potential and all-electron code based on the linearized augmented plane-wave method [64,65]. The implementation of the NL-vdW functionals into WIEN2K has been reported recently [20] and uses the RPS method [16] to evaluate efficiently the NL dispersion energy [Eq. (2)] and the potential $v^{NL}_{c,disp} = \delta E^{NL}_{c,disp}/\delta\rho$ entering into the Kohn-Sham equations. Since the RPS method is based on fast Fourier transforms, it is necessary to smooth the all-electron density ρ around the nuclei; otherwise a plane-wave expansion of ρ in the whole unit cell would be practically impossible. The smooth density that is used for the RPS method is given by

$$\rho_s(\boldsymbol{r}) = \begin{cases} \rho(\boldsymbol{r}), & \rho(\boldsymbol{r}) \leqslant \rho_c, \\ \frac{\rho(\boldsymbol{r}) + A\rho_c[\rho(\boldsymbol{r}) - \rho_c]}{1 + A[\rho(\boldsymbol{r}) - \rho_c]}, & \rho(\boldsymbol{r}) > \rho_c, \end{cases} \quad (5)$$

where $A = 1$ bohr^3 and ρ_c is the density cutoff that determines the degree of smoothness applied to ρ. As discussed in detail in Ref. [20], ρ_c has to be chosen low enough so that the plane-wave expansion of ρ_s is small enough to avoid too expensive fast Fourier transforms. On the other hand, ρ_c should also not be too low; otherwise some accuracy with respect to the calculation with the original density ρ may be lost.

We mention that the WIEN2K calculations with the DRSLL and LMKLL kernels presented in this work (but not those in our previous work [20]) were obtained with the version of these kernels generalized for spin-polarized systems [66], which is relevant for the calculations of the cohesive energy [67] (most atoms are spin polarized) and for bulk Ni that is ferromagnetic. In such spin-polarized cases, Eq. (5) is first applied to the total density $\rho = \rho_\uparrow + \rho_\downarrow$; then the smooth spin-$\sigma$ densities $\rho_{s,\sigma}$ are obtained by multiplying ρ_σ by ρ_s/ρ: $\rho_{s,\sigma} = \rho_\sigma \rho_s/\rho$. The calculations with the functionals of the rVV10 family were done with the non-spin-polarized version of the kernel, since apparently no spin-polarized version has been proposed or used (in particular, the implementation of the rVV10 kernel in the QUANTUM ESPRESSO [34,68] code is non-spin-polarized).

The usual parameters, like the size of the basis set or the number of $\boldsymbol{k}$ points for the integrations in the Brillouin zone, were chosen such that the results are well converged. As in our previous works [27,57,69], the results for the strongly bound solids were obtained non-self-consistently using the PBE orbitals and density; however the self-consistent effects are in general quite small, below 0.005 Å in most cases (the optB88-vdW results from the present work can be compared to those obtained self-consistently in Ref. [20]). The calculations on the weakly bound solids were done self-consistently, except those obtained with MGGA functionals (SCAN, SCAN+rVV10, and TM) that were done non-self-consistently using the PBE orbitals and density since the potential of MGGA functionals is not implemented in WIEN2K.

The list of solids composing our test set can be found in Table I along with their space group. This set consists of 44 solids with (relatively) strong bonding of the metallic, ionic, or covalent type, and 17 solids with weak noncovalent bonding. The strongly bound, rare-gas, and molecular solids have a cubic cell, while the structure of the layered solids is based on the stacking of hexagonal layers. The reference values for the lattice constants and binding energies, to which

TABLE I. The test set of 44 strongly and 17 weakly bound solids. The space group is indicated in parentheses.

Strongly Bound Solids
C ($Fd\bar{3}m$), Si ($Fd\bar{3}m$), Ge ($Fd\bar{3}m$), Sn ($Fd\bar{3}m$), SiC ($F\bar{4}3m$), BN ($F\bar{4}3m$), BP ($F\bar{4}3m$), AlN ($F\bar{4}3m$), AlP ($F\bar{4}3m$), AlAs ($F\bar{4}3m$), GaN ($F\bar{4}3m$), GaP($F\bar{4}3m$), GaAs ($F\bar{4}3m$), InP ($F\bar{4}3m$), InAs ($F\bar{4}3m$), InSb ($F\bar{4}3m$), LiH ($Fm\bar{3}m$), LiF ($Fm\bar{3}m$), LiCl ($Fm\bar{3}m$), NaF ($Fm\bar{3}m$), NaCl ($Fm\bar{3}m$), MgO ($Fm\bar{3}m$), Li ($Im\bar{3}m$), Na ($Im\bar{3}m$), Al ($Fm\bar{3}m$), K ($Im\bar{3}m$), Ca ($Fm\bar{3}m$), Rb ($Im\bar{3}m$), Sr ($Fm\bar{3}m$), Cs ($Im\bar{3}m$), Ba ($Im\bar{3}m$), V ($Im\bar{3}m$), Ni ($Fm\bar{3}m$), Cu ($Fm\bar{3}m$), Nb ($Im\bar{3}m$), Mo ($Im\bar{3}m$), Rh ($Fm\bar{3}m$), Pd ($Fm\bar{3}m$), Ag ($Fm\bar{3}m$), Ta ($Im\bar{3}m$), W ($Im\bar{3}m$), Ir ($Fm\bar{3}m$), Pt ($Fm\bar{3}m$), Au ($Fm\bar{3}m$)
Weakly Bound Solids
Rare gases: Ne ($Fm\bar{3}m$), Ar ($Fm\bar{3}m$), Kr ($Fm\bar{3}m$), Xe ($Fm\bar{3}m$)
Layered solids: graphite ($P6_3/mmc$), h-BN ($P6_3/mmc$), TiS_2 ($P\bar{3}m1$), $TiSe_2$ ($P\bar{3}m1$), MoS_2 ($P6_3/mmc$), $MoSe_2$ ($P6_3/mmc$), $MoTe_2$ ($P6_3/mmc$), $HfTe_2$ ($P\bar{3}m1$), WS_2 ($P6_3/mmc$), WSe_2 ($P6_3/mmc$)
Molecular solids: NH_3 ($P2_13$), CO_2 ($Pa\bar{3}$), $C_6H_{12}N_4$ ($I\bar{4}3m$)

the DFT values will be compared in Sec. III, were obtained either from experiment or from accurate *ab initio* methods. Most of these values, except those for the lattice constant of the molecular solids, are corrected for the thermal and zero-point vibrational effects, such that a direct comparison with our DFT values is possible.

As already mentioned, results for the atomization energy of molecules will also be shown. Our test set is the AE6 set of six molecules (SiH_4, SiO, S_2, C_3H_4, $C_2H_2O_2$, C_4H_8), which were selected to give a fair idea of the accuracy of quantum chemistry methods [70]. Most of the calculations were obtained with the Gaussian augmented plane-wave method as implemented in the CP2K code [71], which allows calculations with NL-vdW functionals [72]. However, since not all functionals are available in CP2K, calculations were also done with the VASP [73] (based on the projector augmented wave method [74]) and deMon (using Gaussian basis functions) codes [75]. We mention that the spin-polarized versions of the DRSLL and LMKLL kernels are not available in the CP2K and VASP codes; therefore the calculations were done with the spin-unpolarized form of the kernels. However, the results were then approximately corrected by adding the spin correction (the difference between the spin- and non-spin-polarized versions of $E_{c,disp}^{NL}$) calculated with the WIEN2K code. Furthermore, since many of our results obtained with NL-vdW functionals for the AE6 test set strongly disagree with those presented in Ref. [76], the VASP results were also used to cross-check the CP2K results (alternatively, WIEN2K could have been used for this purpose).

To finish, we mention that Libxc, a library of exchange-correlation functionals [77,78], has been used for some of the calculations done with the CP2K and WIEN2K codes.

III. RESULTS AND DISCUSSION

A. Strongly bound solids

The results for the equilibrium lattice constant a_0, bulk modulus B_0, and cohesive energy E_{coh} of strongly bound solids obtained with the tested xc functionals are shown in Table II. ME, MAE, MRE, and MARE represent the mean values of the error, absolute error, relative error, and absolute relative error with respect to experiment, respectively, while MAXRE is the maximum relative error. The experimental values were corrected for thermal and zero-point vibrational effects [79,80]. For a few selected functionals, Figs. 3 and 4 show graphically the errors. All detailed results are available in Tables S1–S9 and shown graphically in Figs. S1–S18 of the Supplemental Material [81].

For the lattice constant, the NL-vdW MGGA SCAN+rVV10 and MGGA TM lead to the lowest MAE (0.02 Å) and MARE (0.5%). Without the nonlocal dispersion term, the MAE and MARE with SCAN only slightly increases to 0.03 Å and 0.6%, which are the same values obtained with the GGA PBEsol. Note that other accurate GGA functionals such as SG4 [82] or WC [83] also lead to errors in this range (see Ref. [27]). Interestingly, the ME and MRE for SCAN+rVV10 are basically zero, which means that this functional does not show a particular tendency towards underestimation or overestimation of a_0. Most of the other modern functionals lead to values that are in the range 0.04–0.05 Å for the MAE and 0.8%–1.0% for the MARE. The results obtained with the recent PBEsol+rVV10s can be considered as very accurate and are overall only slightly deteriorated with respect to those obtained with the GGA PBEsol without dispersion correction. As already known from previous studies (see, e.g., Refs. [23,84]), the first two original NL-vdW functionals vdW-DF and vdW-DF2 lead to very large overestimations, similarly as the worst GGAs for solids such as BLYP [47,85] do [27]. This is due to the strong magnitude of the enhancement factors F_{xc} of the corresponding semilocal components (see Fig. 1), which favor too many inhomogeneities in ρ, and therefore too large equilibrium volumes, in the case of solids. rVV10 also shows a clear overestimation of the lattice constant, which is nearly as large as with PBE. From Fig. 1, we can see that the factor F_{xc} is slightly larger in the case of rVV10 than PBE; however the additional nonlocal term in rVV10 reduces the overestimation in a_0.

As expected, the accuracy for the bulk modulus B_0 follows a trend that is rather similar to that for the lattice constant; if a functional is among the most accurate for a_0, then the same conclusion holds also for B_0.

The results for the cohesive energy E_{coh} show that the lowest MAE (0.13 eV/atom) and MARE (3.2%) are obtained with the NL-vdW functional rVV10. Remarkably, these mean errors are smaller than all those obtained with the 62 functionals tested in Ref. [27]. However, the price to pay is to have errors for the lattice constant that are quite large, since the MAE and MARE are more than three times larger than with SCAN+rVV10. Actually, this is a problem that is often encountered with GGAs: a functional that is among the most accurate ones for property A will most likely not be very accurate for another property B that is quite

TABLE II. The ME, MAE, MRE, MARE, and MAXRE with respect to the experimental values (corrected for thermal and zero-point vibrational effects [79,80]) on the testing set of 44 strongly bound solids for the lattice constant a_0, bulk modulus B_0, and cohesive energy E_{coh}. The units of the ME and MAE are Å, GPa, and eV/atom for a_0, B_0, and E_{coh}, respectively, and % for the MRE, MARE, and MAXRE. The solid for which the MAXRE occurs is indicated in parentheses. All results were obtained non-self-consistently using PBE orbitals/density. The functionals are separated into two groups, those that contain a dispersion term (NL or atom-pairwise), and those that do not. Within each group, the functionals are ordered by increasing value of the MARE of a_0.

	a_0					B_0					E_{coh}				
Method	ME	MAE	MRE	MARE	MAXRE	ME	MAE	MRE	MARE	MAXRE	ME	MAE	MRE	MARE	MAXRE
Without dispersion:															
TM	−0.006	0.023	−0.2	0.5	−1.8 (Na)	2.4	6.6	2.1	6.2	25.2 (Cu)	0.24	0.27	6.4	7.0	26.8 (Cu)
SCAN	0.018	0.030	0.3	0.6	3.8 (Cs)	3.5	7.4	−0.4	6.5	−22.0 (Rb)	−0.02	0.19	−0.7	4.9	−16.6 (Cs)
PBEsol	−0.005	0.030	−0.1	0.6	−2.3 (Sr)	0.7	7.8	−1.4	7.0	19.5 (Ni)	0.29	0.31	6.1	6.9	22.8 (Ni)
PBE	0.056	0.061	1.1	1.2	2.8 (Sn)	−11.2	12.2	−9.8	11.0	−25.5 (Ge)	−0.13	0.19	−3.9	5.0	−21.0 (Au)
LDA	−0.071	0.071	−1.5	1.5	−4.9 (Ba)	10.1	11.5	8.1	9.4	32.8 (Ni)	0.77	0.77	17.2	17.2	38.7 (Ni)
With dispersion:															
SCAN+rVV10	0.004	0.022	0.0	0.5	2.5 (Cs)	6.0	8.4	1.8	6.6	22.9 (Cu)	0.11	0.22	2.9	5.4	17.6 (Cu)
PBEsol+rVV10s	−0.019	0.034	−0.4	0.7	−3.0 (Ba)	3.2	8.1	0.9	6.3	22.8 (Ni)	0.45	0.45	10.5	10.6	27.7 (Ni)
C09-vdW	−0.009	0.037	−0.2	0.8	−3.2 (Ba)	0.1	7.7	−0.9	6.5	18.2 (V)	0.27	0.28	5.4	6.7	20.2 (Ni)
vdW-DF-cx	0.015	0.041	0.3	0.9	−2.5 (Ba)	−2.3	8.4	−4.2	8.0	−18.9 (NaF)	0.14	0.19	2.5	4.8	16.8 (Ir)
PBE-D3(BJ)	−0.002	0.042	−0.1	0.9	−3.1 (Li)	−3.1	7.5	−2.1	7.4	−22.6 (Ge)	0.20	0.21	4.8	5.2	15.7 (Ni)
optB86b-vdW	0.015	0.046	0.3	0.9	−2.2 (Sr)	−5.5	8.2	−4.6	7.0	−21.5 (Ge)	0.09	0.16	1.4	4.0	13.6 (Ir)
PBE+rVV10L	0.029	0.045	0.6	0.9	2.1 (Sn)	−6.9	8.9	−5.9	7.8	−21.6 (Ge)	0.10	0.17	2.4	4.1	13.1 (Ni)
rev-vdW-DF2	0.020	0.047	0.4	0.9	−2.1 (Sr)	−6.8	9.0	−5.7	7.8	−23.6 (Ge)	0.02	0.14	−0.9	4.0	−12.3 (Rb)
revPBE-D3(BJ)	−0.011	0.043	−0.4	1.0	−4.8 (Li)	−0.4	8.5	−1.4	8.6	−23.2 (Ge)	0.18	0.21	4.2	5.2	18.7 (Cu)
optB88-vdW	0.026	0.062	0.6	1.3	−2.8 (Cs)	−10.3	11.5	−6.8	9.2	−26.3 (Ge)	−0.04	0.13	−2.0	3.8	−13.4 (Na)
rVV10	0.042	0.083	1.0	1.7	3.4 (Au)	−13.4	14.5	−7.5	10.7	−29.8 (Ge)	0.04	0.13	1.1	3.2	10.4 (Ba)
vdW-DF	0.105	0.106	2.2	2.2	4.6 (Au)	−23.0	23.2	−16.6	17.1	−43.0 (Au)	−0.51	0.51	−12.8	12.8	−32.4 (Au)
vdW-DF2	0.117	0.140	2.5	3.0	6.9 (Au)	−29.4	29.5	−18.2	20.4	−51.7 (Au)	−0.59	0.59	−15.6	15.6	−35.4 (Sr)

different from property A (see also Sec. III C). Also very accurate are optB88-vdW and rev-vdW-DF2 with MAE of 0.13–0.14 eV/atom and MARE in the range 3.8%–4.0%. The results obtained with SCAN+rVV10 (the best one for a_0) are relatively fair, but a certain number of other functionals perform better. We also note the extremely bad performance (strong overestimation) of PBEsol+rVV10s for E_{coh} with MAE and MARE of 0.45 eV/atom and 10.6%, respectively, which makes this functional the fourth worst after LDA, vdW-DF2, and vdW-DF. Actually, as expected and already shown in Ref. [35], PBEsol+rVV10s significantly worsens the cohesive energy with respect to PBEsol, while it was only slightly the case for the lattice constant.

By considering the results in Table II as a whole, an accurate or satisfying description of the three properties seems to be achieved by the following functionals: SCAN, SCAN+rVV10, vdW-DF-cx, PBE-D3(BJ), optB86b-vdW, PBE+rVV10L, and rev-vdW-DF2,

Figures 3 and 4 show the results for the lattice constant and cohesive energy for some of the most recent NL-vdW functionals as well as the MGGAs SCAN and TM. A few interesting observations are the following. The underestimation (overestimation) by PBEsol+rVV10s of the lattice constant (cohesive energy) is particularly pronounced for the alkali and alkaline earth metals. For some of the transition metals, namely Ni, Cu, Rh, Pd, and Ir, PBEsol+rVV10s and TM clearly overestimate E_{coh}. Interestingly, for the lattice constant, PBE+rVV10L and rev-vdW-DF2 lead to very similar results except for the heavy alkali and alkaline earth metals. We note that in general, the difference between the SCAN and SCAN+rVV10 results is quite small, which can be inferred from Fig. 1, where we already observed that the NL-vdW term of SCAN+rVV10 has the smallest magnitude. Finally, we mention that SCAN+rVV10 does not perform well for Cs (strong overestimation of a_0), but leads to rather consistent results for the semiconductors and the transition metals.

B. Weakly bound solids

1. Rare-gas solids

Turning to weakly bound systems, Table III shows the results for the rare-gas solids Ne, Ar, Kr, and Xe, which crystallize in the face-centered cubic structure and have been used in many previous works [27,35,39,57,62,72,76,87–95] for testing functionals since they represent the prototypical van der Waals systems bound by dispersion forces. As criteria to decide what is an (unacceptably) large error with respect to the very accurate CCSD(T) (coupled cluster with singlet, doublet, and perturbative triplet) values [86], we chose 5% and 30% for the relative error on the lattice constant and cohesive energy, respectively.

The results show that only one method, the NL-vdW functional rev-vdW-DF2, leads to no such large errors as defined by our criteria (see also Ref. [76]). The largest error is 3% for a_0 (Ne and Kr) and 19% for E_{coh} (Ne). Another functional that also performs rather well and shows only one large error is the atom-pairwise PBE-D3(BJ), which leads to an overestimation of 42% for E_{coh} of Ne, but below 5% for the others. The

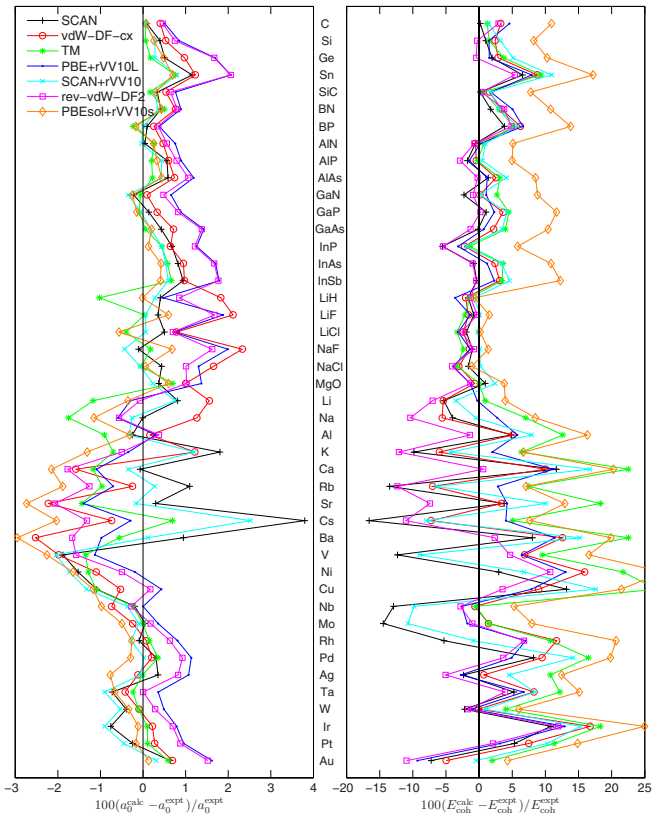

FIG. 3. Relative error (in %) in the calculated lattice constant (left panel) and cohesive energy (right panel) for the 44 strongly bound solids shown for selected functionals.

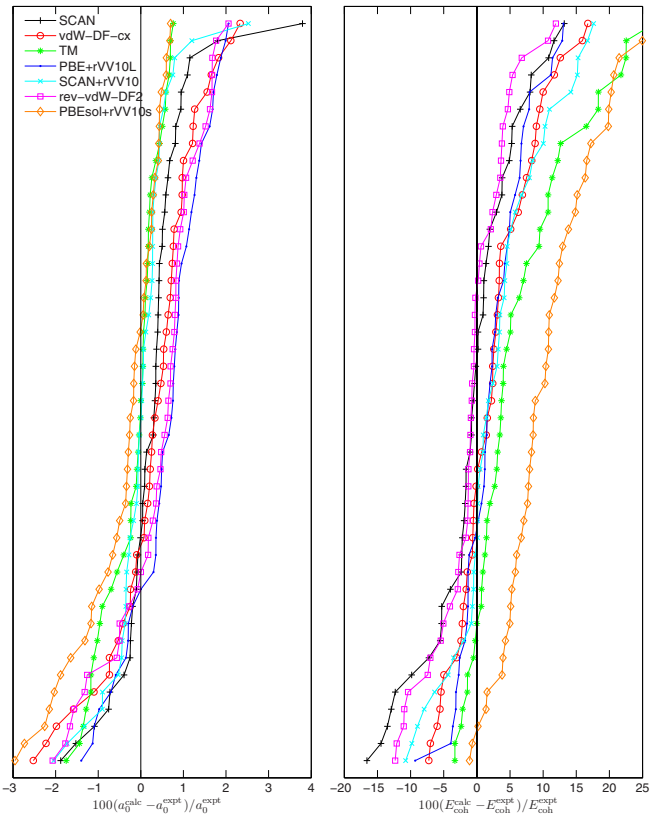

FIG. 4. Same as Fig. 3, but with the difference that for each functional the solids have been ordered such that the relative error goes in the direction of the positive values from bottom to top.

other atom-pairwise functional, revPBE-D3(BJ), leads to very accurate cohesive energy for the four rare gases, but is overall one of the most inaccurate methods for the lattice constant. Somehow satisfying overall, PBEsol+rVV10s leads to errors in the range 35%–40% for the cohesive energy of Ar, Kr, and Xe, but only 10% for Ne.

All other functionals lead to at least one very large error above 50% for $E_{\rm coh}$, including SCAN+rVV10, which performs very badly for Ne for both a_0 and $E_{\rm coh}$, as already noticed in Ref. [39]. Thus, except rev-vdW-DF2, PBE-D3(BJ), and PBEsol+rVV10s, none of the other functionals can be considered as satisfying for rare-gas solids. However, note that other nonhybrid DFT+D3 or DFT+D3(BJ) methods, e.g., PBEsol-D3(BJ) [96] or BLYP-D3 [11], can also be reliable for the rare gases, as shown in our previous work [27]. We can also see that the most accurate methods for a_0, optB88-vdW and optB86b-vdW, which lead to errors not larger than $\sim$1%, are extremely inaccurate for $E_{\rm coh}$ in all cases.

2. *Layered solids*

The hexagonal layered solids constitute another set of prototypical systems bound by weak interactions that is often used for assessing functionals [24–27,35,39,40,55,62,87,88,90,94,97–106]. These systems consist of hexagonal layers that are bound by weak interactions, while the atoms within a layer are strongly bound. The results for the intralayer and interlayer lattice constants a_0 and c_0 as well as the interlayer binding energy E_b are shown in Table IV and compared to results obtained from experiment for a_0 and c_0 or the random-phase approximation (RPA) for E_b [97].

For selected functionals, the results are also compared graphically in Fig. 5. We mention that in the calculation on the monolayer to get E_b, the intralayer lattice constant a was also optimized (results not shown). However, we observed that in the vast majority of cases choosing either $a = a_0^{\rm monolayer}$ or $a = a_0^{\rm bulk}$ for the monolayer has a very small influence, a few tenths of meV/Å^2, on E_b.

The trends observed among the functionals for a_0 are, as expected, similar to those for the strongly bound solids discussed above. In brief, the largest underestimations (up to a few percent) are due to LDA, revPBE-D3(BJ), PBEsol+rVV10s, and C09-vdW, while vdW-DF2 leads to very large overestimations (up to 6%); vdW-DF and rVV10 also show a clear tendency towards overestimation of a_0 (see also Ref. [24]). All other functionals perform clearly better and, as shown in Fig. 5, the most accurate one is SCAN+rVV10, which leads to errors below 0.01 Å (below 0.5%) for all systems. For the interlayer lattice constant c_0, the functionals (beside PBE, which barely binds the layers) that can be identified as more inaccurate than the others are vdW-DF, vdW-DF2, and SCAN, which clearly overestimate c_0, as well as revPBE-D3(BJ), which does the opposite. For these functionals, the error is at least 4% for a certain number

TABLE III. Equilibrium lattice constant a_0 (in Å) and cohesive energy E_{coh} (in meV/atom) of rare-gas solids calculated from various functionals and compared to reference CCSD(T) results [86]. The units of the MRE and MARE are %. The results were obtained from self-consistent calculations, except those for SCAN, SCAN+rVV10, and TM that were obtained using the PBE orbitals/density. The functionals are separated into two groups, those that contain a dispersion term (NL or atom-pairwise), and those that do not. Within each group, the functionals are ordered by increasing MARE. The errors (indicated in parentheses) larger than 5% for a_0 and 30% for E_{coh} are underlined.

Method	Ne	Ar	Kr	Xe	ME	MAE	MRE	MARE
				a_0				
Without dispersion:								
TM	4.05 (−6)	5.23 (0)	5.60 (0)	6.15 (1)	−0.05	0.08	−1.2	1.8
SCAN	4.03 (−6)	5.31 (1)	5.74 (2)	6.33 (4)	0.04	0.18	0.3	3.4
LDA	3.86 (−10)	4.94 (−6)	5.33 (−5)	5.85 (−4)	−0.31	0.31	−6.2	6.2
PBEsol	4.70 (9)	5.88 (12)	6.13 (10)	6.48 (6)	0.49	0.49	9.3	9.3
PBE	4.60 (7)	5.96 (13)	6.42 (15)	7.03 (16)	0.69	0.69	12.7	12.7
With dispersion:								
optB88-vdW	4.26 (−1)	5.23 (0)	5.63 (1)	6.15 (1)	0.01	0.04	0.1	0.7
optB86b-vdW	4.35 (1)	5.32 (1)	5.68 (1)	6.18 (2)	0.07	0.07	1.4	1.4
rVV10	4.21 (−2)	5.16 (−2)	5.52 (−1)	6.01 (−1)	−0.08	0.08	−1.6	1.6
PBEsol+rVV10s	4.41 (3)	5.38 (2)	5.67 (1)	6.08 (0)	0.08	0.08	1.6	1.6
C09-vdW	4.55 (6)	5.34 (2)	5.63 (1)	6.07 (0)	0.09	0.10	2.0	2.1
vdW-DF2	4.17 (−3)	5.28 (1)	5.74 (2)	6.31 (4)	0.07	0.13	1.0	2.4
rev-vdW-DF2	4.42 (3)	5.37 (2)	5.74 (3)	6.22 (2)	0.13	0.13	2.5	2.5
SCAN+rVV10	3.97 (−8)	5.17 (−1)	5.56 (−1)	6.12 (1)	−0.10	0.12	−2.3	2.6
PBE+rVV10L	4.37 (2)	5.48 (4)	5.86 (5)	6.33 (4)	0.20	0.20	3.6	3.6
PBE-D3(BJ)	4.46 (4)	5.49 (5)	5.85 (5)	6.31 (4)	0.22	0.22	4.1	4.1
vdW-DF	4.34 (1)	5.50 (5)	5.95 (6)	6.54 (7)	0.28	0.28	4.9	4.9
vdW-DF-cx	4.40 (2)	5.59 (7)	6.05 (8)	6.53 (7)	0.34	0.34	6.1	6.1
revPBE-D3(BJ)	4.80 (12)	5.67 (8)	5.96 (7)	6.37 (5)	0.39	0.39	7.8	7.8
Reference[a]	4.30	5.25	5.60	6.09				
				E_{coh}				
Without dispersion:								
TM	47 (80)	62 (−30)	82 (−33)	95 (−44)	−30	41	−6.7	46.6
SCAN	54 (107)	61 (−30)	72 (−41)	74 (−56)	−36	50	−5.2	58.7
PBE	19 (−26)	23 (−73)	27 (−78)	29 (−83)	−77	77	−64.9	64.9
PBEsol	12 (−54)	17 (−81)	23 (−81)	32 (−81)	−81	81	−74.4	74.4
LDA	87 (234)	138 (57)	169 (39)	202 (19)	48	48	87.2	87.2
With dispersion:								
revPBE-D3(BJ)	25 (−2)	82 (−7)	126 (3)	192 (13)	5	8	1.7	6.5
rev-vdW-DF2	31 (19)	82 (−7)	111 (−9)	148 (−13)	−9	11	−2.4	12.0
PBE-D3(BJ)	37 (42)	86 (−2)	117 (−4)	162 (−5)	−1	6	7.6	13.1
PBEsol+rVV10s	29 (10)	57 (−35)	75 (−39)	111 (−35)	−34	35	−24.7	29.8
PBE+rVV10L	45 (72)	79 (−10)	102 (−17)	130 (−24)	−13	22	5.4	30.7
rVV10	42 (60)	113 (28)	162 (33)	226 (33)	34	34	38.4	38.4
C09-vdW	51 (98)	118 (34)	156 (28)	212 (25)	33	33	46.1	46.1
vdW-DF2	58 (122)	124 (41)	154 (27)	190 (11)	30	30	50.0	50.0
optB88-vdW	50 (93)	138 (57)	180 (47)	234 (37)	49	49	58.7	58.7
SCAN+rVV10	79 (204)	111 (26)	137 (12)	159 (−7)	20	26	58.9	62.3
optB86b-vdW	61 (134)	137 (56)	174 (42)	224 (32)	47	47	65.9	65.9
vdW-DF-cx	79 (205)	137 (56)	160 (31)	191 (12)	40	40	76.0	76.0
vdW-DF	92 (253)	156 (77)	181 (49)	212 (25)	59	59	100.9	100.9
Reference[a]	26	88	122	170				

[a]The set of CCSD(T) results from Ref. [86] that include the two-, three-, and four-body contributions, but not the effect due to the zero-point vibration.

of solids. The other functionals lead to errors that are at most 3% for all or most solids.

Thus, overall vdW-DF, vdW-DF2, and revPBE-D3(BJ) perform very poorly for both a_0 and c_0. rVV10 is also among the inaccurate methods for a_0, but performs quite well for c_0. As is well known, LDA systematically underestimates the lattice constant, but does it moderately for c_0 since the errors are quite small. Most other dispersion-corrected functionals can be considered as satisfying for both lattice constants. Note that in the work of Björkman [97] optB86b-vdW, vdW-DF-cx, and rev-vdW-DF2 were already shown to be accurate for the lattice constants.

TABLE IV. Equilibrium lattice constants (intralayer a_0 and interlayer c_0, in Å) and interlayer binding energy [E_b, in meV/Å^2, i.e., meV per surface area $A = a_0^2 \cos(\pi/6)$ in the bulk] of layered solids. The units of the MRE and MARE are %. The reference results are from experiment for a_0 and c_0 (with zero-point vibration effect removed) and from RPA calculations for E_b (see Ref. [97]). The results were obtained from self-consistent calculations, except those for SCAN, SCAN+rVV10, and TM that were obtained using the PBE orbitals/density. The functionals are separated into two groups, those that contain a dispersion term (NL or atom-pairwise), and those that do not. Within each group, the functionals are ordered by increasing MARE. The errors (indicated in parentheses) larger than 1% for a_0, 3% for c_0, and 30% for E_b are underlined.

Method	Graphite	h-BN	TiS_2	$TiSe_2$	MoS_2	$MoSe_2$	$MoTe_2$	$HfTe_2$	WS_2	WSe_2	ME	MAE	MRE	MARE
						a_0								
Without dispersion:														
SCAN	2.45 (0)	2.50 (0)	3.42 (0)	3.54 (0)	3.18 (1)	3.30 (0)	3.53 (0)	3.97 (0)	3.17 (1)	3.30 (1)	0.01	0.01	0.2	0.4
TM	2.46 (0)	2.51 (0)	3.38 (−1)	3.50 (−1)	3.15 (0)	3.27 (−1)	3.49 (−1)	3.90 (−1)	3.15 (0)	3.27 (0)	−0.02	0.02	−0.5	0.6
PBE	2.47 (1)	2.51 (0)	3.42 (0)	3.54 (0)	3.19 (1)	3.32 (1)	3.56 (1)	3.98 (1)	3.19 (1)	3.32 (1)	0.02	0.02	0.7	0.7
PBEsol	2.46 (0)	2.50 (0)	3.35 (−2)	3.48 (−2)	3.14 (−1)	3.27 (−1)	3.50 (−1)	3.88 (−2)	3.15 (0)	3.27 (0)	−0.03	0.03	−0.8	0.8
LDA	2.45 (0)	2.49 (−1)	3.31 (−3)	3.43 (−3)	3.12 (−1)	3.25 (−1)	3.47 (−1)	3.82 (−3)	3.13 (−1)	3.25 (−1)	−0.06	0.06	−1.6	1.6
With dispersion:														
SCAN+rVV10	2.45 (0)	2.50 (0)	3.41 (0)	3.54 (0)	3.17 (0)	3.29 (0)	3.52 (0)	3.95 (0)	3.16 (0)	3.29 (0)	0.00	0.01	0.0	0.2
PBE+rVV10L	2.46 (0)	2.51 (0)	3.39 (−1)	3.52 (0)	3.17 (0)	3.30 (0)	3.53 (0)	3.94 (0)	3.17 (1)	3.30 (1)	0.00	0.01	0.1	0.4
optB86b-vdW	2.46 (0)	2.51 (0)	3.38 (−1)	3.52 (0)	3.17 (0)	3.30 (0)	3.53 (0)	3.94 (0)	3.17 (1)	3.30 (1)	0.00	0.01	0.0	0.4
rev-vdW-DF2	2.46 (0)	2.51 (0)	3.39 (−1)	3.52 (0)	3.17 (0)	3.31 (1)	3.54 (1)	3.95 (0)	3.17 (1)	3.30 (1)	0.00	0.01	0.2	0.4
vdW-DF-cx	2.46 (0)	2.51 (0)	3.36 (−1)	3.49 (−1)	3.15 (0)	3.28 (0)	3.51 (0)	3.90 (−1)	3.15 (0)	3.28 (0)	−0.02	0.02	−0.5	0.5
PBE-D3(BJ)	2.46 (0)	2.51 (0)	3.36 (−1)	3.49 (−1)	3.16 (0)	3.28 (0)	3.50 (−1)	3.90 (−1)	3.19 (1)	3.29 (0)	−0.01	0.02	−0.3	0.7
optB88-vdW	2.46 (0)	2.51 (0)	3.41 (0)	3.55 (0)	3.19 (1)	3.32 (1)	3.58 (2)	3.99 (1)	3.19 (1)	3.32 (1)	0.02	0.02	0.7	0.7
C09-vdW	2.46 (0)	2.51 (0)	3.35 (−2)	3.48 (−2)	3.14 (−1)	3.27 (−1)	3.49 (−1)	3.88 (−2)	3.15 (0)	3.27 (0)	−0.03	0.03	−0.8	0.8
revPBE-D3(BJ)	2.47 (1)	2.51 (0)	3.34 (−2)	3.46 (−2)	3.13 (−1)	3.25 (−1)	3.47 (−1)	3.85 (−3)	3.14 (0)	3.26 (−1)	−0.04	0.04	−1.1	1.2
PBEsol+rVV10s	2.46 (0)	2.50 (0)	3.33 (−2)	3.46 (−2)	3.13 (−1)	3.25 (−1)	3.47 (−1)	3.83 (−3)	3.13 (−1)	3.26 (−1)	−0.05	0.05	−1.3	1.3
rVV10	2.47 (1)	2.52 (0)	3.44 (1)	3.58 (1)	3.22 (2)	3.36 (2)	3.60 (2)	4.02 (2)	3.22 (2)	3.36 (2)	0.05	0.05	1.6	1.6
vdW-DF	2.48 (1)	2.52 (0)	3.48 (2)	3.62 (2)	3.24 (2)	3.38 (3)	3.64 (3)	4.08 (3)	3.24 (3)	3.38 (3)	0.08	0.08	2.3	2.3
vdW-DF2	2.48 (1)	2.52 (0)	3.52 (3)	3.68 (4)	3.29 (4)	3.45 (5)	3.72 (6)	4.16 (5)	3.29 (4)	3.44 (5)	0.13	0.13	3.8	3.8
Reference	2.46	2.51	3.41	3.54	3.16	3.29	3.52	3.96	3.15	3.28				
						c_0								
Without dispersion:														
TM	6.63 (0)	6.51 (−2)	5.76 (1)	6.12 (2)	12.5 (2)	13.2 (2)	14.2 (2)	6.75 (2)	12.6 (2)	13.2 (2)	0.2	0.2	1.4	1.7
LDA	6.63 (0)	6.49 (−2)	5.45 (−4)	5.80 (−3)	12.1 (−2)	12.8 (−1)	13.8 (−1)	6.50 (−2)	12.2 (−1)	12.8 (−1)	−0.2	0.2	−1.8	1.8
PBEsol	7.26 (9)	7.06 (6)	5.65 (−1)	5.92 (−1)	12.6 (3)	13.1 (2)	14.0 (0)	6.60 (−1)	12.7 (3)	13.2 (2)	0.2	0.2	2.3	2.9
SCAN	6.95 (5)	6.82 (3)	5.93 (4)	6.32 (5)	12.9 (5)	13.6 (5)	14.7 (5)	6.97 (5)	12.9 (5)	13.6 (5)	0.5	0.5	4.8	4.8
PBE	8.84 (33)	8.69 (31)	6.61 (16)	6.70 (12)	14.8 (21)	15.1 (17)	15.3 (10)	7.21 (9)	14.9 (21)	15.2 (18)	1.7	1.7	18.7	18.7

TABLE IV. (*Continued.*)

Method	Graphite	h-BN	TiS_2	$TiSe_2$	MoS_2	$MoSe_2$	$MoTe_2$	$HfTe_2$	WS_2	WSe_2	ME	MAE	MRE	MARE
With dispersion:														
rev-vdW-DF2	6.64 (0)	6.57 (−1)	5.68 (0)	6.00 (0)	12.4 (1)	13.1 (1)	14.1 (1)	6.71 (1)	12.4 (1)	13.2 (2)	0.1	0.1	0.6	0.9
optB86b-vdW	6.63 (0)	6.53 (−2)	5.69 (0)	6.00 (0)	12.4 (1)	13.1 (1)	14.1 (1)	6.70 (1)	12.5 (1)	13.2 (2)	0.1	0.1	0.5	0.9
vdW-DF-cx	6.56 (−1)	6.45 (−3)	5.61 (−2)	5.93 (−1)	12.3 (0)	12.9 (0)	13.9 (0)	6.60 (−1)	12.4 (1)	13.0 (1)	−0.0	0.1	−0.6	0.9
PBEsol+rVV10s	6.70 (1)	6.60 (−1)	5.54 (−3)	5.87 (−2)	12.2 (−1)	12.9 (0)	13.8 (−1)	6.57 (−1)	12.3 (0)	13.0 (0)	−0.1	0.1	−0.7	0.9
rVV10	6.71 (1)	6.62 (0)	5.70 (0)	6.05 (1)	12.4 (1)	13.1 (2)	14.2 (2)	6.75 (2)	12.5 (1)	13.2 (2)	0.1	0.1	1.1	1.1
C09-vdW	6.46 (−3)	6.35 (−4)	5.55 (−3)	5.89 (−2)	12.2 (−1)	12.8 (0)	13.9 (−1)	6.57 (−1)	12.2 (0)	12.9 (0)	−0.1	0.1	−1.5	1.5
PBE-D3(BJ)	6.79 (2)	6.68 (1)	5.56 (−2)	5.59 (−7)	12.2 (−1)	12.8 (0)	13.8 (−1)	6.58 (−1)	12.2 (0)	12.9 (0)	−0.1	0.1	−1.0	1.6
optB88-vdW	6.69 (1)	6.60 (−1)	5.75 (1)	6.14 (2)	12.5 (2)	13.2 (2)	14.3 (2)	6.80 (2)	12.6 (2)	13.3 (2)	0.2	0.2	1.7	1.8
SCAN+rVV10	6.68 (1)	6.59 (−1)	5.75 (1)	6.22 (4)	12.5 (1)	13.2 (2)	14.3 (2)	6.82 (3)	12.6 (2)	13.2 (2)	0.2	0.2	1.8	1.9
PBE+rVV10L	6.98 (5)	6.88 (4)	5.78 (1)	6.04 (1)	12.6 (2)	13.2 (2)	14.1 (1)	6.71 (1)	12.7 (3)	13.2 (2)	0.2	0.2	2.3	2.3
revPBE-D3(BJ)	6.45 (−3)	6.34 (−4)	5.40 (−5)	5.76 (−4)	11.8 (−4)	12.5 (−3)	13.5 (−3)	6.50 (−2)	11.8 (−4)	12.5 (−3)	−0.3	0.3	−3.6	3.6
vdW-DF2	7.06 (6)	6.99 (5)	5.96 (5)	6.36 (6)	12.9 (5)	13.7 (6)	14.9 (7)	7.07 (6)	13.0 (5)	13.7 (6)	0.6	0.6	5.8	5.8
vdW-DF	7.19 (8)	7.12 (7)	6.11 (7)	6.50 (8)	13.2 (7)	13.9 (7)	15.0 (8)	7.18 (8)	13.2 (7)	13.9 (8)	0.7	0.7	7.7	7.7
Reference	6.63	6.63	5.70	6.00	12.28	12.91	13.96	6.64	12.31	12.95				
						E_b								
Without dispersion:														
LDA	10 (−48)	10 (−30)	20 (7)	21 (24)	13 (−35)	14 (−29)	15 (−26)	19 (3)	13 (−37)	13 (−32)	−4	5	−20.4	27.4
TM	11 (−38)	12 (−19)	13 (−31)	14 (−19)	10 (−50)	11 (−42)	13 (−36)	13 (−28)	10 (−50)	11 (−44)	−7	7	−35.7	35.7
SCAN	7 (−59)	8 (−45)	6 (−68)	6 (−64)	6 (−73)	5 (−72)	7 (−65)	7 (−60)	6 (−72)	5 (−73)	−12	12	−65.2	65.2
PBEsol	2 (−92)	2 (−86)	7 (−62)	10 (−44)	3 (−84)	5 (−75)	8 (−62)	10 (−45)	3 (−86)	4 (−77)	−13	13	−71.4	71.4
PBE	1 (−97)	1 (−96)	1 (−93)	2 (−90)	1 (−97)	1 (−97)	1 (−94)	2 (−90)	1 (−97)	1 (−97)	−18	18	−94.8	94.8
With dispersion:														
SCAN+rVV10	20 (7)	19 (34)	18 (−3)	18 (3)	20 (−3)	19 (−1)	21 (2)	19 (0)	21 (4)	20 (−1)	1	1	4.3	5.8
PBE+rVV10L	15 (−19)	14 (−4)	19 (2)	20 (18)	19 (−6)	20 (2)	22 (4)	20 (6)	19 (−5)	20 (1)	−0	1	−0.1	6.7
vdW-DF2	20 (8)	19 (29)	19 (1)	18 (2)	19 (−6)	18 (−9)	16 (−21)	15 (−19)	19 (−5)	18 (−10)	−1	2	−3.0	10.9
vdW-DF	20 (12)	19 (35)	19 (0)	18 (2)	19 (−7)	18 (−10)	16 (−21)	15 (−18)	19 (−5)	18 (−11)	−1	2	−2.3	12.0
PBEsol+rVV10s	12 (−32)	12 (−20)	20 (7)	21 (21)	17 (−15)	17 (−11)	21 (3)	22 (19)	17 (−14)	17 (−12)	−1	3	−5.4	15.3
rev-vdW-DF2	23 (23)	21 (47)	25 (30)	24 (40)	23 (14)	22 (15)	23 (9)	22 (16)	23 (14)	22 (12)	4	4	22.0	22.0
PBE-D3(BJ)	17 (−9)	16 (9)	27 (45)	30 (72)	24 (17)	26 (34)	30 (44)	27 (46)	26 (28)	28 (38)	6	7	32.5	34.2
vdW-DF-cx	25 (36)	24 (67)	27 (43)	27 (59)	25 (21)	25 (26)	26 (25)	25 (35)	24 (21)	24 (23)	6	6	35.6	35.6
optB88-vdW	27 (47)	26 (80)	27 (45)	26 (52)	26 (28)	25 (29)	24 (16)	23 (23)	26 (29)	25 (27)	7	7	37.5	37.5
optB86b-vdW	27 (47)	26 (80)	28 (48)	28 (60)	26 (29)	26 (31)	26 (24)	25 (33)	26 (30)	26 (28)	7	7	41.0	41.0
rVV10	26 (44)	25 (72)	28 (48)	29 (65)	29 (42)	29 (50)	29 (40)	26 (40)	29 (44)	29 (48)	9	9	49.2	49.2
C09-vdW	29 (59)	28 (96)	32 (72)	33 (88)	30 (44)	29 (49)	30 (44)	30 (59)	29 (44)	29 (45)	11	11	59.9	59.9
revPBE-D3(BJ)	26 (41)	25 (71)	48 (153)	51 (196)	45 (118)	49 (152)	55 (163)	46 (147)	50 (147)	53 (167)	26	26	135.5	135.5
Reference	18.3	14.4	18.8	17.3	20.5	19.6	20.8	18.6	20.2	19.9				

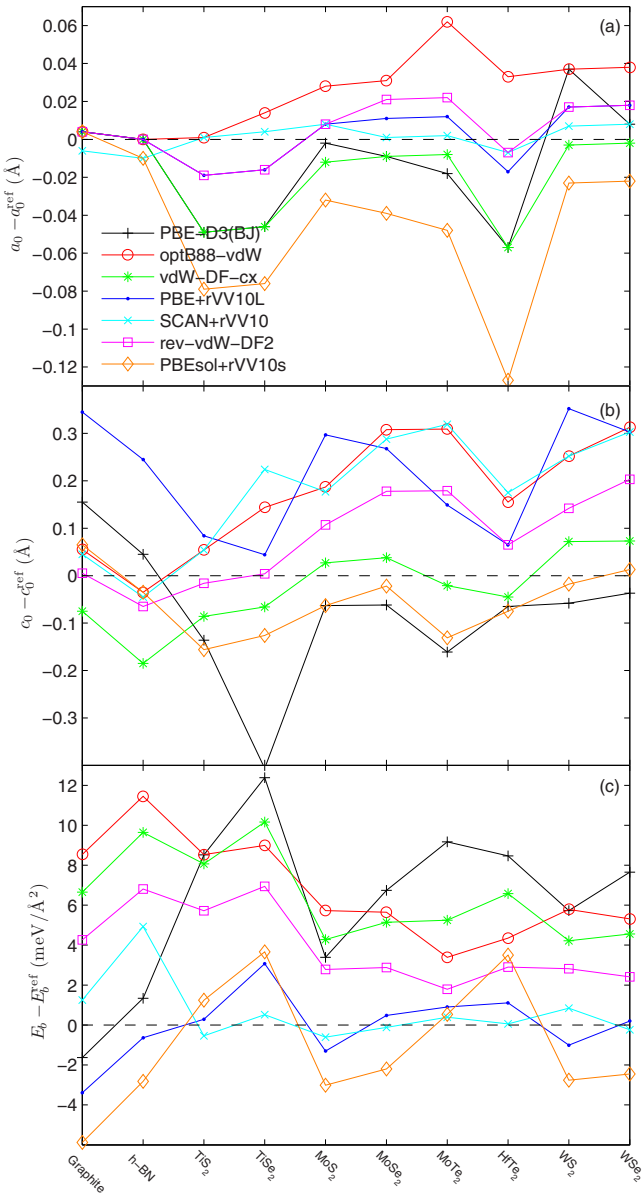

FIG. 5. Error for the intralayer and interlayer lattice constants [in (a) and (b), respectively] and binding energy [(c)] shown for selected functionals.

As observed above for the rare-gas solids, the relative errors for the interlayer binding energy E_b are much larger than for the lattice constants. By considering 30% of relative error as the largest acceptable value for E_b, the results in Table IV show that the functionals that have a reasonable accuracy for all solids except possibly one are SCAN+rVV10, PBE+rVV10L, vdW-DF2, vdW-DF, and PBEsol+rVV10s; rev-vdW-DF2 can also be considered as accurate since for only two solids (h-BN and $TiSe_2$) the relative error is above 30%. Note that the parameter $b = 10$ in the PBE+rVV10L kernel was tuned in order to reproduce at best the RPA results for E_b; therefore its good performance is hardly surprising. The worst functionals are PBE and revPBE-D3(BJ); PBE gives nearly no binding, while revPBE-D3(BJ) overestimates E_b by more than 100% in most cases. Such huge overestimations obtained with revPBE-D3(BJ) have already been observed in the case of adsorption of benzene on transition-metal surfaces [107]. Other very inaccurate functionals are PBEsol, SCAN, C09-vdW, and rVV10 as already shown in Refs. [97,101] for the latter two.

By considering all results for the layered solids, the best functionals are PBE+rVV10L, SCAN+rVV10, and rev-vdW-DF2, since they belong to the accurate methods for a_0, c_0, and E_b at the same time. The results with optB88-vdW and vdW-DF-cx can also be considered as fair. Note the curious performances of vdW-DF and vdW-DF2: very accurate for the interlayer binding energy, but the worst for both lattice constants [101]. For these two functionals, the large contribution of the NL-vdW term to E_b (see Fig. 2) leads to an appropriate binding energy, but the corresponding slope is not steep enough to shorten the lattice constant sufficiently.

We also mention that among a dozen of dispersion-corrected functionals of various families, Tawfik *et al.* [105] concluded that SCAN+rVV10 is overall the most accurate one for a set of twelve layered solids (quite similar to our test set). However, PBE+rVV10L and rev-vdW-DF2 were not considered in their work.

Since results on the layered solids were already available in the literature for many of the functionals, it may be interesting to compare some of them with ours. Peng *et al.* [26,39] reported results for rev-vdW-DF2, PBE+rVV10L, and SCAN+rVV10 that were obtained with VASP. For a_0, their results are in good agreement with ours since they differ by at most 0.01 Å. The agreement for c_0 is relatively good for rev-vdW-DF2 and PBE+rVV10L since the difference is typically below 0.05 Å. A difference of 0.05 Å should be considered as acceptable for such large lattice constants determined by weak interactions. However, with SCAN+rVV10 the disagreement for c_0 is larger (in the range 0.1–0.2 Å), which should be due to self-consistent effects (see discussion in Ref. [27]). Our calculations involving MGGA functionals were done using PBE(+rVV10) for the potential, while those from VASP calculations were probably done self-consistently. The agreement for E_b is good for the three functionals since the discrepancies are below 1 meV/Å^2 in all cases. Considering now the results from Björkman [97] for six functionals (e.g., rev-vdW-DF2 or optB88-vdW) obtained with VASP, the results are also in fair agreement with ours for the lattice constants. However, sizable discrepancies are observed for E_b, since Björkman's results are consistently smaller by 2–3 meV/Å^2 compared to our results, which agree quite well with those from Peng *et al.* [26,39] and Berland and Hyldgaard [25].

3. Molecular solids

Table V shows the results for the equilibrium lattice constant a_0 and lattice energy E_{latt} of the molecular solids NH_3 (ammonia), CO_2 (carbon dioxide), and $C_6H_{12}N_4$ (hexamethylenetetramine). E_{latt} is defined as the difference between the total energy (per molecule) of the crystal and the total energy of one isolated molecule. These three systems, which have a cubic cell, are members of the X23 test set [108] of molecular solids, which is an improvement of the C21 test set [112]. The C21 and X23 sets have been used in a certain number of studies for testing functionals [22,95,108,112–126].

TABLE V. Equilibrium lattice constant a_0 (in Å) and lattice energy E_{latt} (in eV/molecule) of molecular solids calculated from various functionals and compared to experimental results. The results were obtained from self-consistent calculations, except those for SCAN, SCAN+rVV10, and TM that were obtained using the PBE orbitals/density. The functionals are separated into two groups, those that contain a dispersion term (NL or atom-pairwise), and those that do not. Within each group, the functionals are ordered by increasing MARE of E_{latt}. The errors (indicated in parentheses) larger than 3% for a_0 and 15% for E_{latt} are underlined.

	NH_3		CO_2		$C_6H_{12}N_4$	
Method	a_0	E_{latt}	a_0	E_{latt}	a_0	E_{latt}
Without dispersion:						
TM	4.98 (−1)	0.39 (1)	5.49 (−1)	0.25 (−15)	6.86 (−1)	0.68 (−24)
SCAN	4.98 (−1)	0.38 (−3)	5.53 (−1)	0.27 (−8)	6.99 (1)	0.55 (−38)
LDA	4.73 (−6)	0.67 (73)	5.28 (−5)	0.36 (22)	6.72 (−3)	0.90 (1)
PBEsol	4.96 (−2)	0.37 (−4)	5.82 (5)	0.11 (−63)	7.09 (3)	0.32 (−64)
PBE	5.17 (2)	0.29 (−25)	6.07 (9)	0.10 (−66)	7.43 (8)	0.24 (−74)
With dispersion:						
rev-vdW-DF2	5.01 (−1)	0.41 (6)	5.61 (1)	0.27 (−9)	6.92 (0)	0.91 (2)
revPBE-D3(BJ)	5.06 (0)	0.38 (−2)	5.87 (6)	0.27 (−8)	6.96 (1)	0.82 (−8)
vdW-DF-cx	5.07 (0)	0.41 (7)	5.85 (5)	0.32 (10)	7.01 (1)	1.02 (14)
vdW-DF2	5.15 (2)	0.41 (7)	5.61 (1)	0.34 (16)	7.02 (2)	0.97 (9)
SCAN+rVV10	4.89 (−3)	0.44 (15)	5.44 (−2)	0.35 (19)	6.84 (−1)	0.89 (0)
PBE-D3(BJ)	5.02 (−1)	0.43 (13)	5.74 (3)	0.26 (−12)	6.99 (1)	0.81 (−10)
vdW-DF	5.28 (5)	0.38 (0)	5.81 (4)	0.37 (25)	7.16 (4)	1.02 (15)
PBE+rVV10L	5.07 (0)	0.40 (4)	5.74 (3)	0.23 (−23)	7.03 (2)	0.76 (−15)
rVV10	4.96 (−2)	0.47 (23)	5.50 (−1)	0.32 (9)	6.86 (−1)	1.14 (28)
C09-vdW	4.91 (−3)	0.47 (23)	5.53 (−1)	0.33 (13)	6.83 (−1)	1.18 (32)
optB86b-vdW	4.98 (−1)	0.46 (20)	5.58 (0)	0.35 (20)	6.91 (0)	1.17 (31)
PBEsol+rVV10s	4.87 (−4)	0.47 (21)	5.59 (1)	0.20 (−33)	6.89 (0)	0.70 (−22)
optB88-vdW	4.98 (−1)	0.47 (21)	5.53 (−1)	0.37 (26)	6.90 (0)	1.21 (35)
Reference	5.05[a] ($T = 2$ K)	0.39[a]	5.56[b] ($T \sim 5$ K)	0.29[a]	6.91[c] ($T = 34$ K)	0.89[a]

[a]Reference [108]. The values for E_{latt} are corrected for the thermal and zero-point effects.
[b]Reference [109].
[c]References [110,111].

From our results, we can see that most dispersion-corrected functionals except vdW-DF lead to reasonably small errors for the equilibrium lattice constant a_0. Compared to the other dispersion-corrected functionals, SCAN+rVV10 has a more pronounced tendency to underestimate a_0 (−3% for NH_3 and −2% CO_2), while SCAN (and TM) without NL-vdW correction was already pretty good and competes with the best dispersion-corrected functionals. We can see that also PBEsol+rVV10s leads to a large underestimation (−4%) for NH_3. However, we note that the experimental values for a_0 are not corrected for the zero-point vibration effect, which, as mentioned in Ref. [108], may increase the lattice constant by 1%. Thus, a slight underestimation in a_0 should be expected.

For the lattice energy E_{latt}, the most accurate functionals are rev-vdW-DF2 and revPBE-D3(BJ), which lead to errors below 10% for the three systems. However, vdW-DF-cx and vdW-DF2 are also rather accurate, while the most inaccurate functionals are optB88-vdW (see also Ref. [22]), PBEsol+rVV10, and optB86b-vdW, which show errors above 20% for all three molecular solids. Note that, curiously, PBEsol+rVV10 leads to an overestimation for NH_3, but to an underestimation for CO_2 and $C_6H_{12}N_4$.

For this test set of molecular solids, the functional that is overall the most accurate is rev-vdW-DF2. Actually, rev-vdW-DF2 is the most accurate for the lattice constant and the lattice energy. However, in order to be fair, in particular since our test consists of only three systems, we should also mention that other functionals, such as revPBE-D3(BJ), vdW-DF-cx, or vdW-DF2, seem to be pretty accurate overall. The plain MGGAs SCAN and TM lead to large errors only for the lattice energy of $C_6H_{12}N_4$.

Concerning other dispersion-corrected DFT methods, a recent collection of results from the literature for the full X23 test set can be found in Loboda *et al.* [22]. Methods that should be of similar accuracy as the best NL-vdW functionals are for instance B86bPBE+XDM [9,112,127] and PBE+MBD [10,121,128,129], which are both atom-pairwise methods with density-dependent dispersion coefficients.

C. Molecules

All results presented so far were obtained for periodic solids, the focus of the present work. However, as additional information we now provide a snapshot of the accuracy of the functionals for finite systems by considering the atomization energy of molecules. Table VI shows the results obtained for the AE6 test set of six molecules [70].

A well know problem at the GGA level of approximation is the difficulty (and actually the quasi-impossibility) to get with the same functional *very* accurate results for the lattice constants and cohesive energies of strongly bound solids and atomization energies of molecules. In fact, even targeting only

TABLE VI. Atomization energy (in eV) for the molecules of the AE6 test set. The units of the MRE and MARE are %. The reference results are from experiment [70]. The functionals are separated into two groups, those that contain a dispersion term (NL or atom-pairwise), and those that do not. Within each group, the functionals are ordered by increasing MARE. The errors (indicated in parentheses) larger than 5% are underlined.

Method	SiH_4	SiO	S_2	C_3H_4	$C_2H_2O_2$	C_4H_8	ME	MAE	MRE	MARE
Without dispersion:										
SCAN[a]	14.03 (0)	8.02 (−4)	4.73 (7)	30.48 (0)	27.30 (−1)	49.93 (0)	−0.01	0.17	0.5	2.0
TM[b]	13.76 (−2)	8.14 (−2)	4.84 (10)	30.47 (0)	27.69 (1)	49.82 (0)	0.02	0.20	1.1	2.5
PBE[c]	13.58 (−3)	8.50 (2)	4.98 (13)	31.27 (2)	28.84 (5)	50.64 (2)	0.54	0.67	3.5	4.5
PBEsol[c]	14.03 (0)	8.90 (7)	5.36 (22)	32.51 (6)	30.27 (10)	52.85 (6)	1.56	1.56	8.6	8.6
LDA[c]	15.04 (8)	9.70 (16)	5.86 (33)	34.79 (14)	32.75 (19)	56.60 (14)	3.36	3.36	17.3	17.3
With dispersion:										
vdW-DF2[c]	13.94 (0)	8.19 (−2)	4.31 (−2)	29.98 (−2)	27.06 (−1)	48.46 (−3)	−0.44	0.44	−1.7	1.7
vdW-DF[c]	13.91 (−1)	8.04 (−3)	4.40 (0)	29.80 (−3)	26.94 (−2)	48.53 (−3)	−0.49	0.49	−1.9	1.9
SCAN+rVV10[a]	14.04 (0)	8.11 (−3)	4.76 (8)	30.60 (0)	27.61 (1)	50.12 (1)	0.11	0.18	1.2	2.0
revPBE-D3(BJ)[c]	13.51 (−3)	8.18 (−2)	4.79 (9)	30.52 (0)	27.90 (2)	49.63 (0)	−0.00	0.28	0.8	2.6
rVV10[c]	13.52 (−3)	8.43 (1)	4.80 (9)	30.87 (1)	28.31 (3)	49.83 (0)	0.20	0.35	1.8	2.9
optB88-vdW[c]	14.11 (1)	8.49 (2)	4.85 (10)	30.94 (1)	28.37 (3)	50.43 (1)	0.43	0.43	3.1	3.1
vdW-DF-cx[c]	14.11 (1)	8.46 (2)	4.96 (13)	31.05 (2)	28.56 (4)	50.83 (2)	0.57	0.57	3.8	3.8
rev-vdW-DF2[c]	14.15 (1)	8.56 (3)	4.92 (12)	31.35 (3)	28.82 (5)	51.11 (3)	0.72	0.72	4.3	4.3
PBE-D3(BJ)[c]	13.63 (−3)	8.52 (2)	5.01 (14)	31.36 (3)	28.93 (5)	50.85 (2)	0.62	0.74	3.9	4.7
PBE+rVV10L[c]	13.61 (−3)	8.53 (2)	5.02 (14)	31.36 (3)	28.95 (5)	50.84 (2)	0.62	0.75	3.9	4.8
optB86b-vdW[a]	14.06 (1)	8.68 (4)	5.11 (16)	31.11 (2)	28.92 (5)	50.79 (2)	0.68	0.68	4.9	4.9
C09-vdW[c]	14.18 (1)	8.62 (3)	5.07 (15)	31.53 (3)	29.10 (6)	51.56 (3)	0.91	0.91	5.4	5.4
PBEsol+rVV10s[c]	14.06 (1)	8.92 (7)	5.39 (22)	32.59 (7)	30.36 (11)	53.01 (6)	1.62	1.62	8.9	8.9
Reference	13.98	8.33	4.41	30.56	27.46	49.83				

[a]Calculated with VASP.
[b]Calculated with deMon non-self-consistently using PBE orbitals/density.
[c]Calculated with CP2K.

two of these three properties seems unachievable, and the results in Refs. [51,130–133] illustrate this problem for the lattice constant of solids and atomization energy of molecules. For this it is necessary to use functionals from higher rungs of Jacob's ladder, MGGAs or hybrids, to get accurate results for both properties simultaneously [50,52,79,131,134]. As seen in Table VI, the dispersion-corrected GGA functionals have the same problems as the GGA, which is expected since adding a dispersion term to a functional should in principle have a rather limited effect on the results for strongly bound systems (in particular if a dispersion term of small magnitude such as some of those of the rVV10-type is used; see Fig. 2). Indeed, the five most accurate GGA-based functionals for the atomization energy (MAE below 0.5 eV), namely vdW-DF2, vdW-DF, revPBE-D3(BJ), rVV10, and optB88-vdW, are also the worst for the lattice constant a_0 (see Table II). The reverse is also true: some of the most accurate NL-vdW GGAs for a_0, e.g., C09-vdW or PBEsol+rVV10s, lead to the worst results for the AE6 atomization energy with a MAE that is several times larger than for vdW-DF and vdW-DF2. However, note that vdW-DF-cx is rather well balanced since it is reasonably accurate for both the lattice constant and the molecular atomization energy.

As mentioned, a dispersion term in the functional should be of relatively small importance for covalently bound systems. Thus, as for the strongly bound solids (Sec. III A) some of the trends in the results correlate well with the GGA enhancement factors F_{xc} shown in Fig. 1. The factors F_{xc} with the largest magnitude (vdW-DF and vdW-DF2) lead to the best results, while a reduction of the magnitude of F_{xc} leads to more and more overbinding, like PBEsol(+rVV10s) and ultimately LDA.

Thus, a GGA-based functional cannot be among the best methods for more than one of the three properties, which are the lattice constant and cohesive energy of solids and the atomization energy of molecules. MGGA functionals can alleviate this problem as exemplified by SCAN(+rVV10), which belongs (more or less) to the most accurate functionals for *all three properties*. As shown in Table VI, SCAN and SCAN+rVV10 (but also TM) lead to MAE below 0.2 eV and were competing with the best GGA functionals for strongly bound solids (the only clear exceptions are the GGAs optB88-vdW and rVV10, which are better for E_{coh}; see Sec. III A).

We mention that results for the AE6 molecules obtained with several NL-vdW functionals were already available [76]. Table S10 of the Supplemental Material [81] compares our results obtained with two codes (CP2K and VASP) with those from Ref. [76] obtained with VASP. (To make the comparison possible, our vdW-DF2, optB88-vdW, and rev-vdW-DF2 results in Table S10 were obtained using the non-spin-polarized version of the DRSLL and LMKLL kernels.) The agreement between our two sets of results is in general very good, which gives us confidence about the reliability of our results. However, the agreement with the values from Ref. [76] is good only in the case of PBE and rev-vdW-DF2 (except for C_4H_8 with the latter functional). In the case of vdW-DF2 and optB88-vdW extremely large discrepancies are systematically obtained, the worst being for

SiH_4 with vdW-DF2 (8.9 eV from Ref. [76] and 14.2 eV in the present work with both codes).

IV. DISCUSSION AND CONCLUSION

A dozen of dispersion-corrected functionals have been tested on periodic solids and the goal was to identify which of them are the most appropriate for solids. In particular, the question is whether there is a dispersion-corrected functional that is reasonably accurate for all types of systems that have been considered in the present work. The test set consisted of strongly and weakly bound solids, and for the latter group three classes were considered: rare gases, layered solids, and molecular solids. Additionally, results on a small set of molecules were also shown.

Our results are summarized in Fig. 6. For the strongly bound solids, the functionals that were considered as giving satisfying results for all properties (lattice constant, bulk modulus, and cohesive energy) are the MGGA SCAN and the NL-vdW SCAN+rVV10, PBE+rVV10L, optB86b-vdW, rev-vdW-DF2, and vdW-DF-cx. The atom-pairwise methods PBE-D3(BJ) and revPBE-D3(BJ) are also quite accurate.

In the case of the rare-gas solids, rev-vdW-DF2 and PBE-D3(BJ) are the most accurate overall (lattice constant and cohesive energy). The results on the hexagonal layered solids have shown that only three functionals provide reasonably small errors for all properties (intralayer and interlayer lattice constants and interlayer binding energy) and for most solids: PBE+rVV10L, SCAN+rVV10, and rev-vdW-DF2; however, none of them is clearly superior to the two others. Finally, for the molecular solids, rev-vdW-DF2 and revPBE-D3(BJ) lead overall to the smallest errors for the lattice constant and cohesive energy.

From this summary the conclusion is the following: rev-vdW-DF2 is among the most accurate methods for all three classes of weakly bound solids and is therefore a recommended functional for treating weak interactions in solids. Remarkably, rev-vdW-DF2 leads to no single catastrophic results, at least not in our test set of systems with weak interactions. This functional does not belong to the list of the top-performing functionals for strongly bound interactions; however the results are actually relatively fair overall: although not among the best for the lattice constant it is still better than PBE, and excellent for the cohesive energy. Thus, overall rev-vdW-DF2 seems to be a very good compromise for solid-state calculations and, furthermore, it is not based on a MGGA functional but on a GGA, which leads to practical advantages. MGGA functionals lead to more expensive calculations [55,135] and may require denser grids for integrations as observed for SCAN [118,136]. However, the advantage of MGGA functionals is to be generally more accurate as shown again in the present work for molecules. It is worth mentioning that very recently, Fischer *et al.* [137] showed that rev-vdW-DF2 is one of the most accurate functionals (among fourteen dispersion-corrected ones) for the structural and energetic properties of a set of sixteen SiO_2 and $AlPO_4$ frameworks. Thus, this consolidates the conclusion of the present work.

We finish by mentioning that the recently proposed PBEsol+rVV10s functional shows mixed performances.

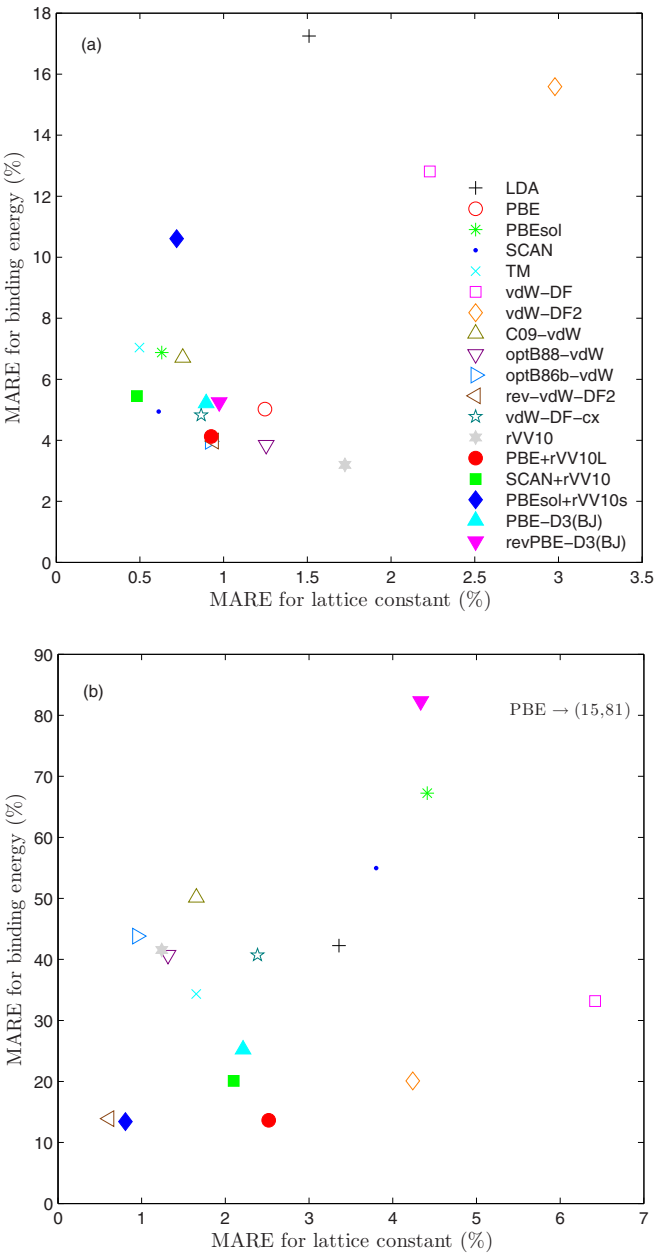

FIG. 6. MARE for lattice constant versus MARE for binding energy for (a) the 44 strongly bound solids and (b) the 17 weakly bound solids [(a_0, E_{coh}) of the rare-gas solids, (a_0, E_{latt}) of the molecular solids, and (c_0, E_b) of the layered solids].

While it is one of the most accurate for the lattice constant of weakly bound solids [see Fig. 6(b)], it is not recommended for the cohesive energy of strongly bound and molecular solids.

ACKNOWLEDGMENTS

This work was supported by Projects No. F41 (SFB ViCoM) and No. P27738-N28 of the Austrian Science Fund (FWF) and by the TU-D doctoral college (TU Wien). Part of this work was granted access to the HPC resources of [TGCC/CINES/IDRIS] under Allocation No. 2017-A0010907682 made by GENCI. We are grateful to Ferenc Karsai for help regarding VASP calculations.

[1] H. Rydberg, M. Dion, N. Jacobson, E. Schröder, P. Hyldgaard, S. I. Simak, D. C. Langreth, and B. I. Lundqvist, Phys. Rev. Lett. **91**, 126402 (2003).

[2] M. Dion, H. Rydberg, E. Schröder, D. C. Langreth, and B. I. Lundqvist, Phys. Rev. Lett. **92**, 246401 (2004); **95**, 109902(E) (2005).

[3] T. Thonhauser, V. R. Cooper, S. Li, A. Puzder, P. Hyldgaard, and D. C. Langreth, Phys. Rev. B **76**, 125112 (2007).

[4] D. C. Langreth, B. I. Lundqvist, S. D. Chakarova-Käck, V. R. Cooper, M. Dion, P. Hyldgaard, A. Kelkkanen, J. Kleis, L. Kong, S. Li, P. G. Moses, E. Murray, A. Puzder, H. Rydberg, E. Schröder, and T. Thonhauser, J. Phys.: Condens. Matter **21**, 084203 (2009).

[5] P. Hyldgaard, K. Berland, and E. Schröder, Phys. Rev. B **90**, 075148 (2014).

[6] K. Berland, V. R. Cooper, K. Lee, E. Schröder, T. Thonhauser, P. Hyldgaard, and B. I. Lundqvist, Rep. Prog. Phys. **78**, 066501 (2015).

[7] P. Hohenberg and W. Kohn, Phys. Rev. **136**, B864 (1964).

[8] W. Kohn and L. J. Sham, Phys. Rev. **140**, A1133 (1965).

[9] A. D. Becke and E. R. Johnson, J. Chem. Phys. **122**, 154104 (2005).

[10] A. Tkatchenko and M. Scheffler, Phys. Rev. Lett. **102**, 073005 (2009).

[11] S. Grimme, J. Antony, S. Ehrlich, and H. Krieg, J. Chem. Phys. **132**, 154104 (2010).

[12] S. Grimme, A. Hansen, J. G. Brandenburg, and C. Bannwarth, Chem. Rev. **116**, 5105 (2016).

[13] J. Hermann, R. A. DiStasio, Jr., and A. Tkatchenko, Chem. Rev. **117**, 4714 (2017).

[14] J. P. Perdew, K. Burke, and M. Ernzerhof, Phys. Rev. Lett. **77**, 3865 (1996); **78**, 1396 (1997).

[15] K. Choudhary, G. Cheon, E. Reed, and F. Tavazza, Phys. Rev. B **98**, 014107 (2018).

[16] G. Román-Pérez and J. M. Soler, Phys. Rev. Lett. **103**, 096102 (2009).

[17] R. Sabatini, E. Küçükbenli, B. Kolb, T. Thonhauser, and S. de Gironcoli, J. Phys.: Condens. Matter **24**, 424209 (2012).

[18] J. Wu and F. Gygi, J. Chem. Phys. **136**, 224107 (2012).

[19] A. H. Larsen, M. Kuisma, J. Löfgren, Y. Pouillon, P. Erhart, and P. Hyldgaard, Modell. Simul. Mater. Sci. Eng. **25**, 065004 (2017).

[20] F. Tran, J. Stelzl, D. Koller, T. Ruh, and P. Blaha, Phys. Rev. B **96**, 054103 (2017).

[21] J. Klimeš, D. R. Bowler, and A. Michaelides, J. Phys.: Condens. Matter **22**, 022201 (2010).

[22] O. A. Loboda, G. A. Dolgonos, and A. D. Boese, J. Chem. Phys. **149**, 124104 (2018).

[23] J. Klimeš, D. R. Bowler, and A. Michaelides, Phys. Rev. B **83**, 195131 (2011).

[24] T. Björkman, Phys. Rev. B **86**, 165109 (2012).

[25] K. Berland and P. Hyldgaard, Phys. Rev. B **89**, 035412 (2014).

[26] H. Peng and J. P. Perdew, Phys. Rev. B **95**, 081105(R) (2017).

[27] F. Tran, J. Stelzl, and P. Blaha, J. Chem. Phys. **144**, 204120 (2016).

[28] J. P. Perdew and K. Schmidt, AIP Conf. Proc. **577**, 1 (2001).

[29] S. Grimme, S. Ehrlich, and L. Goerigk, J. Comput. Chem. **32**, 1456 (2011).

[30] A. D. Becke, J. Chem. Phys. **98**, 1372 (1993).

[31] A. D. Becke, J. Chem. Phys. **98**, 5648 (1993).

[32] O. A. Vydrov and T. Van Voorhis, Phys. Rev. Lett. **103**, 063004 (2009).

[33] O. A. Vydrov and T. Van Voorhis, J. Chem. Phys. **133**, 244103 (2010).

[34] R. Sabatini, T. Gorni, and S. de Gironcoli, Phys. Rev. B **87**, 041108(R) (2013).

[35] A. V. Terentjev, L. A. Constantin, and J. M. Pitarke, Phys. Rev. B **98**, 214108 (2018).

[36] K. Lee, E. D. Murray, L. Kong, B. I. Lundqvist, and D. C. Langreth, Phys. Rev. B **82**, 081101(R) (2010).

[37] J. Aragó, E. Ortí, and J. C. Sancho-García, J. Chem. Theory Comput. **9**, 3437 (2013).

[38] N. Mardirossian and M. Head-Gordon, Phys. Chem. Chem. Phys. **16**, 9904 (2014).

[39] H. Peng, Z.-H. Yang, J. P. Perdew, and J. Sun, Phys. Rev. X **6**, 041005 (2016).

[40] I. Hamada, Phys. Rev. B **89**, 121103(R) (2014); **91**, 119902(E) (2015).

[41] K. Berland, Y. Jiao, J.-H. Lee, T. Rangel, J. B. Neaton, and P. Hyldgaard, J. Chem. Phys. **146**, 234106 (2017).

[42] Y. Jiao, E. Schröder, and P. Hyldgaard, J. Chem. Phys. **148**, 194115 (2018).

[43] Y. Zhang and W. Yang, Phys. Rev. Lett. **80**, 890 (1998).

[44] S. H. Vosko, L. Wilk, and M. Nusair, Can. J. Phys. **58**, 1200 (1980).

[45] J. P. Perdew and Y. Wang, Phys. Rev. B **45**, 13244 (1992); **98**, 079904(E) (2018).

[46] V. R. Cooper, Phys. Rev. B **81**, 161104(R) (2010).

[47] A. D. Becke, Phys. Rev. A **38**, 3098 (1988).

[48] A. D. Becke, J. Chem. Phys. **85**, 7184 (1986).

[49] J. P. Perdew and Y. Wang, Phys. Rev. B **33**, 8800 (1986).

[50] J. Sun, A. Ruzsinszky, and J. P. Perdew, Phys. Rev. Lett. **115**, 036402 (2015).

[51] J. P. Perdew, A. Ruzsinszky, G. I. Csonka, O. A. Vydrov, G. E. Scuseria, L. A. Constantin, X. Zhou, and K. Burke, Phys. Rev. Lett. **100**, 136406 (2008); **102**, 039902(E) (2009).

[52] J. Tao and Y. Mo, Phys. Rev. Lett. **117**, 073001 (2016).

[53] Y. Mo, R. Car, V. N. Staroverov, G. E. Scuseria, and J. Tao, Phys. Rev. B **95**, 035118 (2017).

[54] E. B. Isaacs and C. Wolverton, Phys. Rev. Mater. **2**, 063801 (2018).

[55] D. Mejia-Rodriguez and S. B. Trickey, Phys. Rev. B **98**, 115161 (2018).

[56] G.-X. Zhang, A. M. Reilly, A. Tkatchenko, and M. Scheffler, New J. Phys. **20**, 063020 (2018).

[57] F. Tran, P. Kovács, L. Kalantari, G. K. H. Madsen, and P. Blaha, J. Chem. Phys. **149**, 144105 (2018).

[58] S. Jana, A. Patra, and P. Samal, J. Chem. Phys. **149**, 044120 (2018).

[59] S. Jana, K. Sharma, and P. Samal, J. Chem. Phys. **149**, 164703 (2018).

[60] Y. Zhang, D. A. Kitchaev, J. Yang, T. Chen, S. T. Dacek, R. A. Sarmiento-Pérez, M. A. L. Marques, H. Peng, G. Ceder, J. P. Perdew, and J. Sun, npj Comput. Mater. **4**, 9 (2018).

[61] K. T. Lundgaard, J. Wellendorff, J. Voss, K. W. Jacobsen, and T. Bligaard, Phys. Rev. B **93**, 235162 (2016).

[62] A. V. Terentjev, P. Cortona, L. A. Constantin, J. M. Pitarke, F. Della Sala, and E. Fabiano, Computation **6**, 7 (2018).

[63] P. Blaha, K. Schwarz, G. K. H. Madsen, D. Kvasnicka, J. Luitz, R. Laskowski, F. Tran, and L. D. Marks, *WIEN2K: An*

Augmented Plane Wave plus Local Orbitals Program for Calculating Crystal Properties (Vienna University of Technology, Austria, 2018).
[64] O. K. Andersen, Phys. Rev. B **12**, 3060 (1975).
[65] D. J. Singh and L. Nordström, *Planewaves, Pseudopotentials, and the LAPW Method*, 2nd ed. (Springer, New York, 2006).
[66] T. Thonhauser, S. Zuluaga, C. A. Arter, K. Berland, E. Schröder, and P. Hyldgaard, Phys. Rev. Lett. **115**, 136402 (2015).
[67] L. Gharaee, P. Erhart, and P. Hyldgaard, Phys. Rev. B **95**, 085147 (2017).
[68] P. Giannozzi, O. Andreussi, T. Brumme, O. Bunau, M. Buongiorno Nardelli, M. Calandra, R. Car, C. Cavazzoni, D. Ceresoli, M. Cococcioni, N. Colonna, I. Carnimeo, A. Dal Corso, S. de Gironcoli, P. Delugas, R. A. DiStasio, Jr., A. Ferretti, A. Floris, G. Fratesi, G. Fugallo, R. Gebauer, U. Gerstmann, F. Giustino, T. Gorni, J. Jia, M. Kawamura, H.-Y. Ko, A. Kokalj, E. Küçükbenli, M. Lazzeri, M. Marsili, N. Marzari, F. Mauri, N. L. Nguyen, H.-V. Nguyen, A. Otero-de-la-Roza, L. Paulatto, S. Poncé, D. Rocca, R. Sabatini, B. Santra, M. Schlipf, A. P. Seitsonen, A. Smogunov, I. Timrov, T. Thonhauser, P. Umari, N. Vast, X. Wu, and S. Baroni, J. Phys.: Condens. Matter **29**, 465901 (2017).
[69] P. Kovács, F. Tran, P. Blaha, and G. K. H. Madsen, J. Chem. Phys. **150**, 164119 (2019).
[70] B. J. Lynch and D. G. Truhlar, J. Phys. Chem. A **107**, 8996 (2003); **108**, 1460 (2004).
[71] J. VandeVondele, M. Krack, F. Mohamed, M. Parrinello, T. Chassaing, and J. Hutter, Comput. Phys. Commun. **167**, 103 (2005).
[72] F. Tran and J. Hutter, J. Chem. Phys. **138**, 204103 (2013); **139**, 039903 (2013).
[73] G. Kresse and J. Furthmüller, Phys. Rev. B **54**, 11169 (1996).
[74] P. E. Blöchl, Phys. Rev. B **50**, 17953 (1994).
[75] M. E. Casida, C. Daul, A. Goursot, A. Köster, L. G. M. Pettersson, E. Proynov, A. St-Amant, D. R. Salahub, S. Chrétien, H. Duarte, N. Godbout, J. Guan, C. Jamorski, M. Leboeuf, V. Malkin, O. Malkina, M. Nyberg, L. Pedocchi, F. Sim, and A. Vela, *deMon-KS Version 3.5, deMon Software* (University of Montreal, 1998).
[76] M. Callsen and I. Hamada, Phys. Rev. B **91**, 195103 (2015); **95**, 039905(E) (2017).
[77] M. A. L. Marques, M. J. T. Oliveira, and T. Burnus, Comput. Phys. Commun. **183**, 2272 (2012).
[78] S. Lehtola, C. Steigemann, M. J. T. Oliveira, and M. A. L. Marques, SoftwareX **7**, 1 (2018).
[79] L. Schimka, J. Harl, and G. Kresse, J. Chem. Phys. **134**, 024116 (2011).
[80] K. Lejaeghere, V. Van Speybroeck, G. Van Oost, and S. Cottenier, Crit. Rev. Solid State Mater. Sci. **39**, 1 (2014).
[81] See Supplemental Material at http://link.aps.org/supplemental/10.1103/PhysRevMaterials.3.063602 for the detailed results for the lattice constant, bulk modulus, and cohesive energy of the 44 strongly bound solids, and comparison of the atomization energies of the molecules of the AE6 test set obtained with different codes.
[82] L. A. Constantin, A. Terentjevs, F. Della Sala, P. Cortona, and E. Fabiano, Phys. Rev. B **93**, 045126 (2016).
[83] Z. Wu and R. E. Cohen, Phys. Rev. B **73**, 235116 (2006).
[84] J. Park, B. D. Yu, and S. Hong, Curr. Appl. Phys. **15**, 885 (2015).
[85] C. Lee, W. Yang, and R. G. Parr, Phys. Rev. B **37**, 785 (1988).
[86] K. Rościszewski, B. Paulus, P. Fulde, and H. Stoll, Phys. Rev. B **62**, 5482 (2000).
[87] F. Ortmann, F. Bechstedt, and W. G. Schmidt, Phys. Rev. B **73**, 205101 (2006).
[88] F. Tran, R. Laskowski, P. Blaha, and K. Schwarz, Phys. Rev. B **75**, 115131 (2007).
[89] J. Harl and G. Kresse, Phys. Rev. B **77**, 045136 (2008).
[90] P. Haas, F. Tran, and P. Blaha, Phys. Rev. B **79**, 085104 (2009); **79**, 209902(E) (2009).
[91] K. E. Yousaf and E. N. Brothers, J. Chem. Theory Comput. **6**, 864 (2010).
[92] T. Bučko, J. Hafner, S. Lebègue, and J. G. Ángyán, J. Phys. Chem. A **114**, 11814 (2010).
[93] W. A. Al-Saidi, V. K. Voora, and K. D. Jordan, J. Chem. Theory Comput. **8**, 1503 (2012).
[94] T. Bučko, S. Lebègue, J. Hafner, and J. G. Ángyán, Phys. Rev. B **87**, 064110 (2013).
[95] J. Moellmann and S. Grimme, J. Phys. Chem. C **118**, 7615 (2014).
[96] L. Goerigk and S. Grimme, Phys. Chem. Chem. Phys. **13**, 6670 (2011).
[97] T. Björkman, J. Chem. Phys. **141**, 074708 (2014).
[98] M. Hasegawa and K. Nishidate, Phys. Rev. B **70**, 205431 (2004).
[99] M. Hasegawa, K. Nishidate, and H. Iyetomi, Phys. Rev. B **76**, 115424 (2007).
[100] T. Björkman, A. Gulans, A. V. Krasheninnikov, and R. M. Nieminen, Phys. Rev. Lett. **108**, 235502 (2012).
[101] T. Björkman, A. Gulans, A. V. Krasheninnikov, and R. M. Nieminen, J. Phys.: Condens. Matter **24**, 424218 (2012).
[102] G. Graziano, J. Klimeš, F. Fernandez-Alonso, and A. Michaelides, J. Phys.: Condens. Matter **24**, 424216 (2012).
[103] C. R. C. Rêgo, L. N. Oliveira, P. Tereshchuk, and J. L. F. Da Silva, J. Phys.: Condens. Matter **27**, 415502 (2015); **28**, 129501 (2016).
[104] I. V. Lebedeva, A. V. Lebedev, A. M. Popov, and A. A. Knizhnik, Comput. Mater. Sci. **128**, 45 (2017).
[105] S. A. Tawfik, T. Gould, C. Stampfl, and M. J. Ford, Phys. Rev. Mater. **2**, 034005 (2018).
[106] I. Mosyagin, D. Gambino, D. G. Sangiovanni, I. A. Abrikosov, and N. M. Caffrey, Phys. Rev. B **98**, 174103 (2018).
[107] W. Reckien, M. Eggers, and T. Bredow, Beilstein J. Org. Chem. **10**, 1775 (2014).
[108] A. M. Reilly and A. Tkatchenko, J. Chem. Phys. **139**, 024705 (2013).
[109] Y. N. Heit, K. D. Nanda, and G. J. O. Beran, Chem. Sci. **7**, 246 (2016).
[110] L. N. Becka and D. W. J. Cruickshank, Proc. R. Soc. A **273**, 435 (1963).
[111] K. Berland and P. Hyldgaard, J. Chem. Phys. **132**, 134705 (2010).
[112] A. Otero-de-la-Roza and E. R. Johnson, J. Chem. Phys. **137**, 054103 (2012).
[113] A. M. Reilly and A. Tkatchenko, J. Phys. Chem. Lett. **4**, 1028 (2013).

[114] T. Bučko, S. Lebègue, J. Hafner, and J. G. Ángyán, J. Chem. Theory Comput. **9**, 4293 (2013).
[115] D. J. Carter and A. L. Rohl, J. Chem. Theory Comput. **10**, 3423 (2014).
[116] L. Kronik and A. Tkatchenko, Acc. Chem. Res. **47**, 3208 (2014).
[117] J. Hoja, A. M. Reilly, and A. Tkatchenko, WIREs Comput. Mol. Sci. **7**, e1294 (2017).
[118] J. G. Brandenburg, J. E. Bates, J. Sun, and J. P. Perdew, Phys. Rev. B **94**, 115144 (2016).
[119] J. G. Brandenburg, E. Caldeweyher, and S. Grimme, Phys. Chem. Chem. Phys. **18**, 15519 (2016).
[120] M. Cutini, B. Civalleri, M. Corno, R. Orlando, J. G. Brandenburg, L. Maschio, and P. Ugliengo, J. Chem. Theory Comput. **12**, 3340 (2016).
[121] J. Hermann and A. Tkatchenko, J. Chem. Theory Comput. **14**, 1361 (2018).
[122] S. P. Thomas, P. R. Spackman, D. Jayatilaka, and M. A. Spackman, J. Chem. Theory Comput. **14**, 1614 (2018).
[123] G. A. Dolgonos, O. A. Loboda, and A. D. Boese, J. Phys. Chem. A **122**, 708 (2018).
[124] M. Mortazavi, J. G. Brandenburg, R. J. Maurer, and A. Tkatchenko, J. Phys. Chem. Lett. **9**, 399 (2018).
[125] J. G. Brandenburg, C. Bannwarth, A. Hansen, and S. Grimme, J. Chem. Phys. **148**, 064104 (2018).
[126] L. M. LeBlanc, J. A. Weatherby, A. Otero-de-la-Roza, and E. R. Johnson, J. Chem. Theory Comput. **14**, 5715 (2018).
[127] E. R. Johnson, in *Non-Covalent Interactions in Quantum Chemistry and Physics: Theory and Applications*, edited by A. Otero-de-la-Roza and G. A. DiLabio (Elsevier, Amsterdam, 2017), p. 169.
[128] A. Tkatchenko, R. A. DiStasio, Jr., R. Car, and M. Scheffler, Phys. Rev. Lett. **108**, 236402 (2012).
[129] A. Ambrosetti, A. M. Reilly, R. A. DiStasio, Jr., and A. Tkatchenko, J. Chem. Phys. **140**, 18A508 (2014).
[130] Y. Zhao and D. G. Truhlar, J. Chem. Phys. **128**, 184109 (2008).
[131] J. P. Perdew, A. Ruzsinszky, G. I. Csonka, L. A. Constantin, and J. Sun, Phys. Rev. Lett. **103**, 026403 (2009); **106**, 179902 (2011).
[132] E. Fabiano, L. A. Constantin, and F. Della Sala, Phys. Rev. B **82**, 113104 (2010).
[133] P. Haas, F. Tran, P. Blaha, and K. Schwarz, Phys. Rev. B **83**, 205117 (2011).
[134] F. Della Sala, E. Fabiano, and L. A. Constantin, Int. J. Quantum Chem. **116**, 1641 (2016).
[135] A. V. Bienvenu and G. Knizia, J. Chem. Theory Comput. **14**, 1297 (2018).
[136] Y. Yao and Y. Kanai, J. Chem. Phys. **146**, 224105 (2017).
[137] M. Fischer, W. J. Kim, M. Badawi, and S. Lebègue, J. Chem. Phys. **150**, 094102 (2019).